nature cancer

ARTICLES

https://doi.org/10.1038/s43018-022-00426-6

Check for updates

Cancer-associated fibroblasts employ NUFIP1-dependent autophagy to secrete nucleosides and support pancreatic tumor growth

Meng Yuan[1,2,9], Bo Tu[3,4,9], Hengchao Li[5,9], Huanhuan Pang[6,9], Nan Zhang[1], Minghe Fan[1], Jingru Bai[1], Wei Wang[7], Zhaoqi Shu[1], Christopher C. DuFort[4], Sihan Huo[1], Jie Zhai[1], Ke Yao[5], Lina Wang[1], Haoqiang Ying[3], Wei-Guo Zhu[2,8], Deliang Fu[5]✉, Zeping Hu[6]✉ and Ying Zhao[1]✉

Cancer-associated fibroblasts (CAFs) are one of the most prominent and active components in the pancreatic tumor microenvironment. Our data show that CAFs are critical for survival from pancreatic ductal adenocarcinoma (PDAC) on glutamine deprivation. Specifically, we uncovered a role for nucleosides, which are secreted by CAFs through autophagy in a nuclear fragile X mental retardation-interacting protein 1 (NUFIP1)-dependent manner, increased glucose utilization and promoted growth of PDAC. Moreover, we demonstrate that CAF-derived nucleosides induced glucose consumption under glutamine-deprived conditions and displayed a dependence on *MYC*. Using an orthotopic mouse model of PDAC, we found that inhibiting nucleoside secretion by targeting NUFIP1 in the stroma reduced tumor weight. This finding highlights a previously unappreciated metabolic network within pancreatic tumors in which diverse nutrients are used to promote growth in an austere tumor microenvironment.

PDAC is characterized by widespread fibrotic desmoplasia, among which CAFs are one of the most critical stromal cells that promote tumor growth and metastasis, and contribute to treatment resistance[1,2]. CAFs are mainly derived from quiescent pancreatic stellate cells (PSCs)[3]. It has been reported that autophagy, a process of lysosome-dependent protein degradation[4,5], is required for the transition of PSCs to CAFs, during which interleukin-6 and extracellular matrix molecules are produced to promote tumor proliferation and metastasis[6]. PSC autophagy also produces alanine, which acts as an alternative carbon source to fuel the tricarboxylic acid (TCA) cycle in PDAC, thus attenuating the dependence of PDAC on glucose and serum-derived nutrients[7]. Moreover, blocking autophagy in CAFs could support chemotherapy by inhibiting the proliferation of pancreatic cancer[8]. The critical role of autophagy in the tumor microenvironment has also been observed in other tumor models. For example, in squamous cell carcinoma, CAF autophagy machinery is required for activation because it is associated with an increase of effector gene expression[9]. High-mobility group box 1 (HMGB1) cytokines secreted by CAFs through autophagy-based secretion are involved in maintaining the stemness of luminal breast cancer cells[10]. The importance of autophagy in the stromal microenvironment is clear; however, the specific roles of autophagy in CAFs need further exploration.

Autophagy was formerly considered a nonselective degradation pathway. Recent studies have reported the selective autophagic degradation of several organelles, including mitochondria, peroxisomes, ribosomes, endoplasmic reticulum (ER) and the nucleus, under various conditions[11,12]. Ribophagy is a ribosome degradation process mediated by a specific cargo receptor NUFIP1 (ref [13]). In our study, we show that NUFIP1-mediated ribosomal RNA degradation in CAFs is critical for PDAC growth under glutamine deprivation through the secretion of nucleosides. Mechanistically, we describe nucleosides promoting glucose consumption by activating the *MYC* pathway, suggesting a metabolic network within the pancreatic tumor microenvironment.

Results

CAFs promote growth of PDAC in NUFIP1-dependent manner. Glutamine and glucose are important for PDAC cancer cells because they are two major carbon and nitrogen sources for tumor growth and proliferation[14–16]. Both glucose and glutamine in tumor interstitial fluid (TIF) from orthotopic syngeneic graft model were decreased relative to plasma (Fig. 1a,b). By using human PDAC (hPADC) and murine PDAC (mPADC, from C57Bl/6J isogenic tetO_LKras^{G12D}p53$^{L/+}$p48-Cre, termed 14837T and 14838T) cell lines, we observed that some PDAC cell lines (8988T, 8988S, PL45 and MIA Paca-2) are more sensitive to glutamine depletion than to glucose depletion (Extended Data Fig. 1a). To confirm the importance of glutamine metabolism in PDAC, we treated PDAC cells with the glutaminase (GLS) inhibitor 968. GLS is the first required enzyme for mitochondrial glutamine anaplerosis. Notably, PDAC cells were significantly sensitive to GLS inhibition (Extended Data Fig. 1b). Next, we implanted the highly 968 sensitive 14837T cell line into the pancreas of mice and treated with 968. However, by

[1]Beijing Key Laboratory of Protein Posttranslational Modifications and Cell Function, Department of Biochemistry and Molecular Biology, School of Basic Medical Sciences, Peking University Health Science Center, Beijing, China. [2]Marshall Laboratory of Biomedical Engineering, Shenzhen University School of Medicine, Shenzhen, China. [3]Molecular and Cellular Oncology Department, University of Texas MD Anderson Cancer Center, Houston, TX, USA. [4]Clinical Research Division, Fred Hutchinson Cancer Research Center, Seattle, WA, USA. [5]Department of Pancreatic Surgery, Huashan hospital, Institute of Pancreatic Disease, FuDan University, Shanghai, China. [6]School of Pharmaceutical Sciences, Tsinghua-Peking Joint Center for Life Sciences, Beijing Frontier Research Center for Biological Structure, Tsinghua University, Beijing, China. [7]Department of Immunology, School of Basic Medical Sciences, Peking University, NHC Key Laboratory of Medical Immunology, Beijing, China. [8]Department of Biochemistry and Molecular Biology, School of Medicine, Shenzhen University, Shenzhen, China. [9]These authors contributed equally: Meng Yuan, Bo Tu, Hengchao Li, Huanhuan Pang. ✉e-mail: surgeonfu@163.com; zeping_hu@mail.tsinghua.edu.cn; zhaoying0812@bjmu.edu.cn

using this orthotopic model, we were surprised to find that GLS inhibition had no effect on tumor growth (Fig. 1c).

Given the inconsistent results in vitro and in vivo, we suspected that the stroma of PDAC may play a role in sustaining tumor growth when glutamine metabolism is inhibited. As CAFs are considered one of the most abundant stromal cells, we tested whether CAFs could support PDAC growth under glutamine deprivation. The importance of CAF autophagy in the metabolic support of pancreatic cancer has been reported before[7]. To further explore the role of selective autophagy in CAF-induced proliferation, *ATG3/ATG5* or receptors of ER-phagy (*Sec24c*), mitophagy (*Parkin*) or ribophagy (*NUFIP1*) were separately knocked out in a human CAF (hCAF) line and a mouse CAF (mCAF) line. We observed that autophagy, especially ribophagy, but not other forms of selective autophagy, had an impact on proliferation of PDAC grown under glutamine-free conditions or after treatment with a GLS inhibitor (Fig. 1d–g and Extended Data Fig. 1c,d), whereas NUFIP1 knockout (KO) had no effect on CAF viability (Extended Data Fig. 1e). Similar results were also observed in PDAC patient-derived tumor cell lines (Fig. 1h,i). To further validate the role of ribophagy, we used a Trp35Ala mouse NUFIP1 mutant (Trp40 in human) (Fig. 1j), which shows defects in ribophagy and interaction with LC3 (ref. [13]). When expressed in NUFIP1-null cells, only wild-type (WT) NUFIP1, but not the Trp35Ala mutant, restored the capacity of NUFIP1-null mCAFs to sustain PDAC proliferation on glutamine depletion (Fig. 1k,l and Extended Data Fig. 1f), indicating that stromal ribophagy may play a role in PDAC maintenance.

Ribosomal RNA degradation is activated in CAFs. Given the possible role of CAF ribophagy in PDAC, we then tested the status of ribophagy in CAFs. We found that the degradation of 28S/18S rRNA was induced by glutamine starvation in CAFs, but not in PDAC, indicating that NUFIP1-dependent rRNA degradation is highly activated in CAFs (Fig. 2a–d and Extended Data Fig. 2a–h). In addition, rRNA degradation is highly dependent on autophagy because the degradation is impaired in *ATG3* KO cells (Fig. 2e and Extended Data Fig. 2i–k). Ribosomes are a complex consisting of rRNA and about 80 ribosomal proteins (r-proteins). Therefore, we next tested the r-protein levels in CAFs. We found that certain r-proteins were reduced by glutamine starvation in CAFs (Fig. 2f). However, NUFIP1 was not required for the reduction of these r-proteins (Fig. 2g), which is consistent with a recent report[17], suggesting that NUFIP1 mediated rRNA degradation but not r-protein degradation in CAFs. As previously reported, NUFIP1 is an RNA-binding protein[18]. By performing RIP (RNA-binding protein immunoprecipitation)–reverse transcription (RT)–PCR analysis, we found that NUFIP1 also binds to 5S, 5.8S, 28S and 18S rRNA (Fig. 2h and Extended Data Fig. 2l). However, it cannot be co-immunoprecipitated with r-protein (Extended Data Fig. 2m), indicating that NUFIP1 may not interact with the entire ribosome. To further prove that glutamine deprivation impacts rRNA stability but not rRNA production, we used actinomycin D to block transcription and then detected rRNA levels. Consistent with our previous observations, knocking out NUFIP1 markedly protected rRNA from degradation in the presence or absence of actinomycin D (Fig. 2i, j and Extended Data Fig. 2n,o), suggesting that NUFIP1 may play an important role in regulating rRNA degradation.

We then explored the potential mechanism by which rRNA degradation is activated only in CAFs. Glutamine deprivation did not change the total cellular amount of NUFIP1 in CAFs or in PDAC, so we hypothesized that its subcellular localization may be affected. Indeed, on glutamine starvation NUFIP1 translocated from the nucleus to the cytoplasm in CAFs, but not in PDAC (Fig. 2k,l and Extended Data Fig. 3a,b). Imaging studies also confirmed that NUFIP1 translocated from the nucleus to lysosomal-associated membrane protein 1 (LAMP1) and LC3-positive autophagosomes in CAFs (Fig. 2m,n and Extended Data Fig. 3c,d). Moreover, we purified autophagosome from *Stx17*-KO CAFs in which autophagosome–lysosome fusion was blocked[19]. Indeed, the autophagosome accumulation of rRNA was fully suppressed by NUFIP1 impairment (Fig. 2o,p and Extended Data Fig. 3e), indicating NUFIP1's role in translocation of rRNA to autophagosome.

The inhibition of mammalian target of rapamycin complex 1 (mTORC1) increased the association between NUFIP1 and ribosomes[13]. We then tested the mTORC1 activity measured by phosphorylation of S6K (Thr389). As shown in Fig. 2q,r, p-S6K was suppressed by glutamine starvation in CAFs but not in PDAC. The mTORC1 pathway can by activated by oncogenic *KRAS* mutations, which are present in >90% of cases of PDAC[20]. In the doxycycline-inducible $KRAS^{G12D}$-expressing cell line 14837T, we also found that p-S6K levels are decreased whereas NUFIP1 translocation increased on glutamine starvation in the absence of doxycycline (*KRAS*-off) (Fig. 2s,t), indicating the important role of $KRAS^{G12D}$ in the mTORC1 pathway and the regulation of NUFIP1.

CAFs secrete nucleosides dependent on NUFIP1. As nucleosides can be derived from lysosomal rRNA turnover, we next tested the metabolites that were secreted by CAFs. A drop in the levels of both intracellular nucleosides and secreted nucleosides was observed when NUFIP1 and autophagy were impaired in CAFs (Fig. 3a,b and Extended Data Fig. 4a–f). However, there is no significant difference of amino acid secretion activity between WT CAFs and *NUFIP1*-KO CAFs (Extended Data Fig. 4g). To demonstrate that CAF-derived nucleosides were taken up by PDAC cells, we performed metabolite tracing experiments in which CAFs were grown in medium containing [$^{13}C_6$]glucose to label secreted nucleosides. The conditioned medium (CM) from the labeled cells was then added to PDAC cells. We found that labeled nucleosides were produced and secreted by

Fig. 1 | CAFs promote growth of PDAC in an NUFIP1-dependent manner. a,**b**, The 14837T cells orthotopically injected into C57BL/6J mice. After 14 d, the plasma and TIF of mice were taken out, and the concentrations of glucose (**a**) and glutamine (**b**) were measured ($n = 6$ mice). Data are shown as mean ± s.d. Pairwise comparisons were conducted using two-tailed, unpaired Student's *t*-tests. Ctr, control. **c**, The 14837T cells orthotopically injected into mice and 968 (5 mg kg d^{-1}) injected intraperitoneally from day 5. After 14 d, the tumors were weighed ($n = 6$ mice). Data are shown as mean ± s.d. Statistical analysis was performed as in **b**. **d**,**e**, Cells counted to calculate the cell proliferation. The cells were incubated in complete medium or CM from different cell lines for 48 h (**d**). Two different sgRNA sequences were used to knock-out NUFIP1(**e**). Data are shown as mean ± s.d. ($n = 4$ independent samples). **f**, Schematic of the experiments depicted in **e** and **g**. **g**, PDAC cells co-cultured with different CAFs in a transwell chamber for 48 h with or without 968. The PDAC cells were counted to calculate the cell proliferation. Data are shown as mean ± s.d. ($n = 4$ independent samples). **h**, Human pancreatic cancer, PDAC-1 and PDAC-2, incubated in CM from different cell lines for 48 h. The cells were counted to calculate the cell proliferation. Data are shown as mean ± s.d. ($n = 4$ independent samples). **i**, PDAC-1 and PDAC-2 co-cultured with different CAF cells in a transwell chamber for 48 h with or without 968. The PDAC cells were counted to calculate the cell proliferation. Data are shown as mean ± s.d. ($n = 4$ independent samples). **j**, Schematic diagram of NUFIP1 amino acid sequence. **k**, CRISPR–Cas9-resistant NUFIP1-WT(r) and NUFIP1-W35A(r) overexpressed in NUFIP1-KO mCAFs. Western blotting was then performed to determine NUFIP1 protein levels. The results represent $n = 3$ independent experiments. **l**, Cell proliferation of 14837T cells treated with CM (no glutamine) from 14837T, mCAF (NUFIP1-WT(r)), mCAF (NUFIP1-KO) and mCAF (NUFIP1-W35A(r)) cells. Data are shown as mean ± s.d. ($n = 4$ independent samples). Statistical analysis was performed using ordinary one-way ANOVA with Tukey's multiple comparisons test (**d**,**e**,**g**–**i**,**l**).

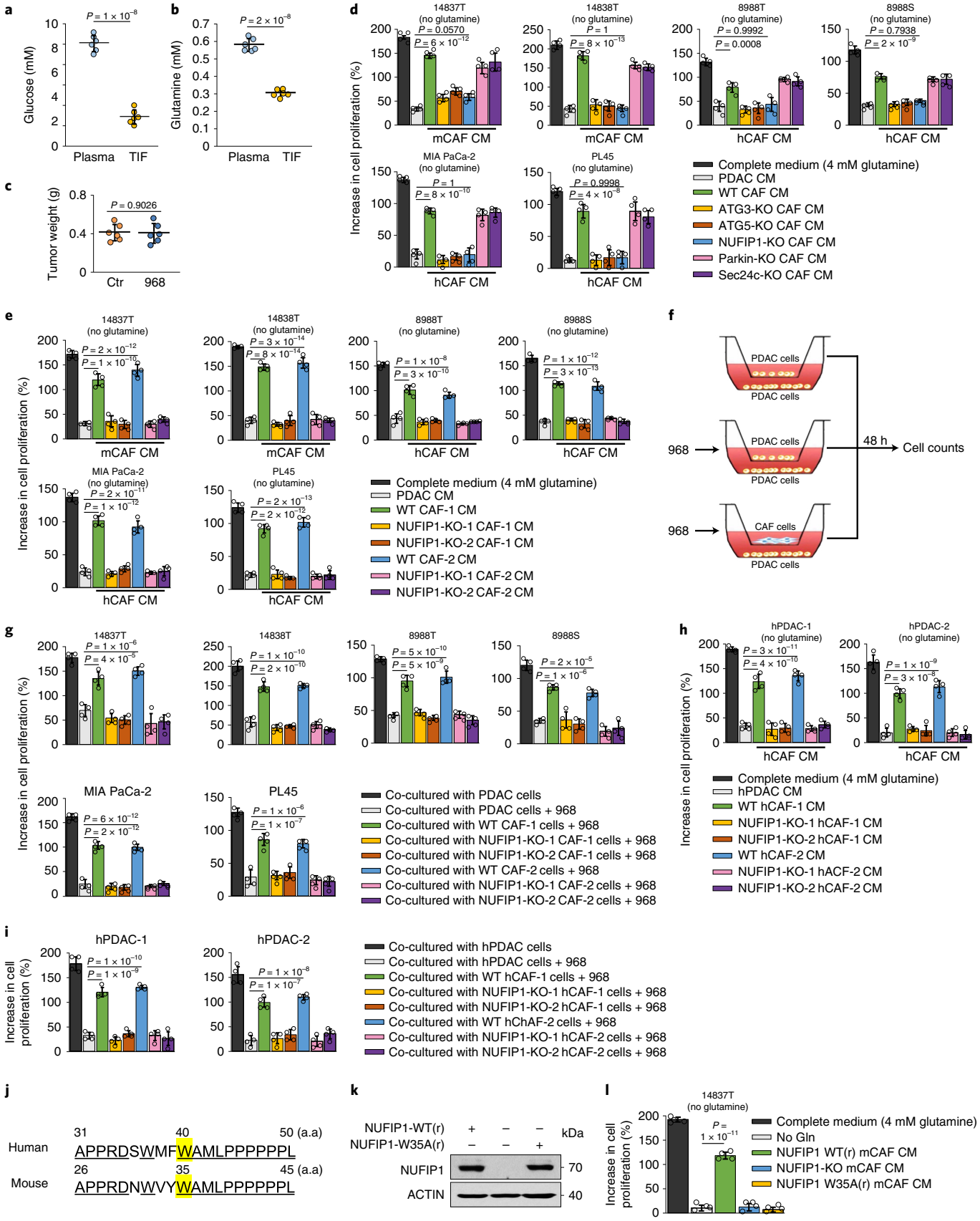
a
Glucose (mM)
P = 1 × 10−8
Plasma
TIF
b
Glutamine (mM)
P = 2 × 10−8
Plasma
TIF
c
Tumor weight (g)
P = 0.9026
Ctr
968
d
Increase in cell proliferation (%)
14837T (no glutamine)
P = 0.0570
P = 6 × 10−12
14838T (no glutamine)
P = 1
P = 8 × 10−13
8988T (no glutamine)
P = 0.9992
P = 0.0008
8988S (no glutamine)
P = 0.7938
P = 2 × 10−9
MIA PaCa-2 (no glutamine)
P = 1
P = 8 × 10−10
PL45 (no glutamine)
P = 0.9998
P = 4 × 10−8
mCAF CM
hCAF CM
Complete medium (4 mM glutamine)
PDAC CM
WT CAF CM
ATG3-KO CAF CM
ATG5-KO CAF CM
NUFIP1-KO CAF CM
Parkin-KO CAF CM
Sec24c-KO CAF CM
e
Increase in cell proliferation (%)
14837T (no glutamine)
P = 2 × 10−12
P = 1 × 10−10
14838T (no glutamine)
P = 3 × 10−14
P = 8 × 10−14
8988T (no glutamine)
P = 1 × 10−8
P = 3 × 10−10
8988S (no glutamine)
P = 1 × 10−12
P = 3 × 10−13
MIA PaCa-2 (no glutamine)
P = 2 × 10−11
P = 1 × 10−12
PL45 (no glutamine)
P = 2 × 10−13
P = 2 × 10−12
mCAF CM
hCAF CM
Complete medium (4 mM glutamine)
PDAC CM
WT CAF-1 CM
NUFIP1-KO-1 CAF-1 CM
NUFIP1-KO-2 CAF-1 CM
WT CAF-2 CM
NUFIP1-KO-1 CAF-2 CM
NUFIP1-KO-2 CAF-2 CM
f
PDAC cells
PDAC cells
968
PDAC cells
PDAC cells
48 h
Cell counts
968
CAF cells
PDAC cells
g
Increase in cell proliferation (%)
14837T
P = 1 × 10−6
P = 4 × 10−5
14838T
P = 1 × 10−10
P = 2 × 10−10
8988T
P = 5 × 10−10
P = 5 × 10−9
8988S
P = 2 × 10−5
P = 1 × 10−6
MIA PaCa-2
P = 6 × 10−12
P = 2 × 10−12
PL45
P = 1 × 10−6
P = 1 × 10−7
Co-cultured with PDAC cells
Co-cultured with PDAC cells + 968
Co-cultured with WT CAF-1 cells + 968
Co-cultured with NUFIP1-KO-1 CAF-1 cells + 968
Co-cultured with NUFIP1-KO-2 CAF-1 cells + 968
Co-cultured with WT CAF-2 cells + 968
Co-cultured with NUFIP1-KO-1 CAF-2 cells + 968
Co-cultured with NUFIP1-KO-2 CAF-2 cells + 968
h
Increase in cell proliferation (%)
hPDAC-1 (no glutamine)
P = 3 × 10−11
P = 4 × 10−10
hPDAC-2 (no glutamine)
P = 1 × 10−9
P = 3 × 10−8
hCAF CM
Complete medium (4 mM glutamine)
hPDAC CM
WT hCAF-1 CM
NUFIP1-KO-1 hCAF-1 CM
NUFIP1-KO-2 hCAF-1 CM
WT hCAF-2 CM
NUFIP1-KO-1 hACF-2 CM
NUFIP1-KO-2 hCAF-2 CM
i
Increase in cell proliferation (%)
hPDAC-1
P = 1 × 10−10
P = 1 × 10−9
hPDAC-2
P = 1 × 10−8
P = 1 × 10−7
Co-cultured with hPDAC cells
Co-cultured with hPDAC cells + 968
Co-cultured with WT hCAF-1 cells + 968
Co-cultured with NUFIP1-KO-1 hCAF-1 cells + 968
Co-cultured with NUFIP1-KO-2 hCAF-1 cells + 968
Co-cultured with WT hChAF-2 cells + 968
Co-cultured with NUFIP1-KO-1 hCAF-2 cells + 968
Co-cultured with NUFIP1-KO-2 hCAF-2 cells + 968
j
Human
31
40
50 (a.a)
APPRDSWMFWAMLPPPPPPL
Mouse
26
35
45 (a.a)
APPRDNWVYWAMLPPPPPPL
k
NUFIP1-WT(r)
NUFIP1-W35A(r)
kDa
NUFIP1
70
ACTIN
40
l
Increase in cell proliferation (%)
14837T (no glutamine)
P = 1 × 10−11
Complete medium (4 mM glutamine)
No Gln
NUFIP1 WT(r) mCAF CM
NUFIP1-KO mCAF CM
NUFIP1 W35A(r) mCAF CM

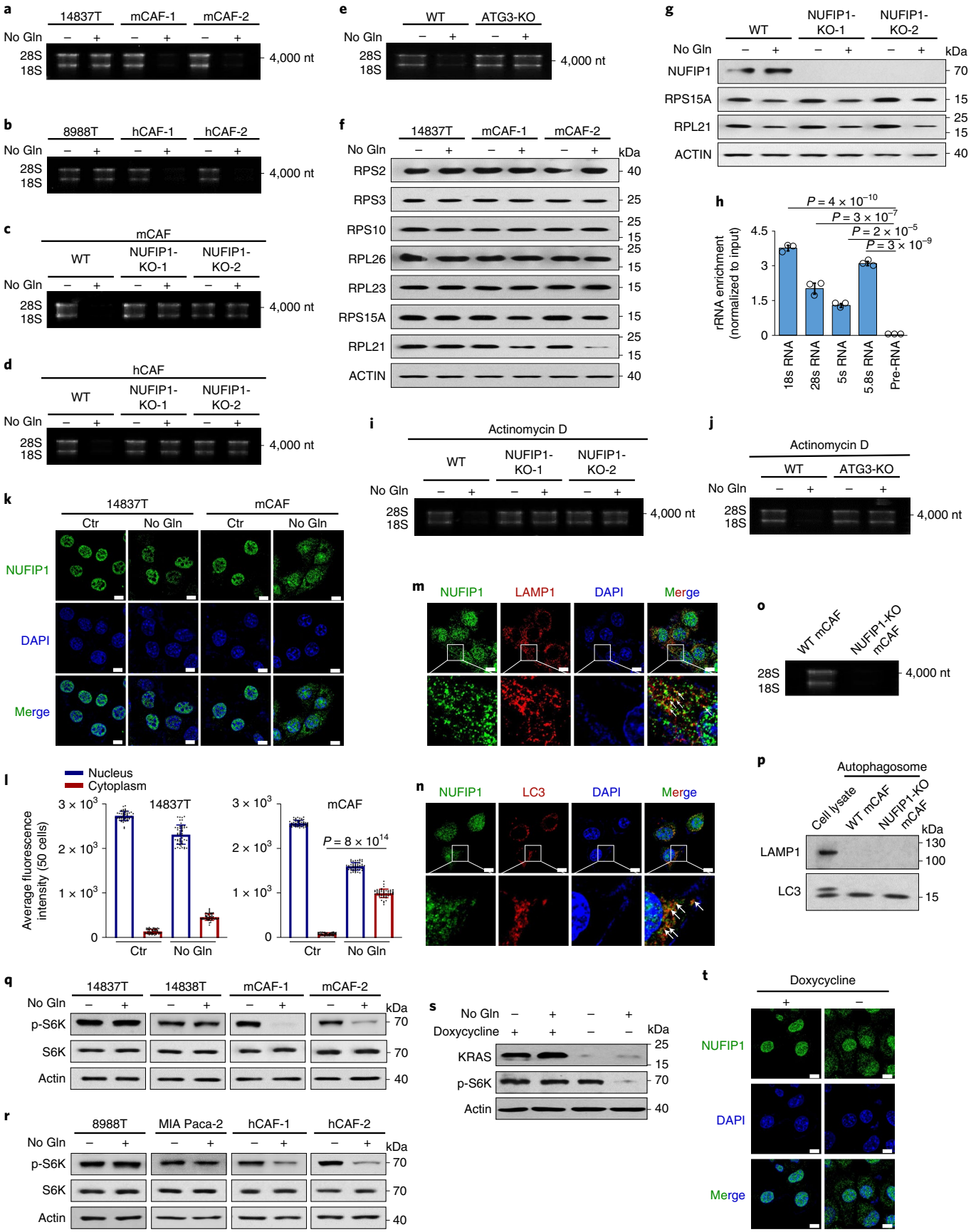
a
14837T
mCAF-1
mCAF-2
No Gln
28S
18S
4,000 nt
b
8988T
hCAF-1
hCAF-2
c
mCAF
WT
NUFIP1-KO-1
NUFIP1-KO-2
d
hCAF
e
WT
ATG3-KO
f
RPS2
RPS3
RPS10
RPL26
RPL23
RPS15A
RPL21
ACTIN
kDa
g
NUFIP1
RPS15A
RPL21
ACTIN
h
P = 4 × 10−10
P = 3 × 10−7
P = 2 × 10−5
P = 3 × 10−9
rRNA enrichment (normalized to input)
18s RNA
28s RNA
5s RNA
5.8s RNA
Pre-RNA
i
Actinomycin D
j
k
Ctr
No Gln
NUFIP1
DAPI
Merge
l
Nucleus
Cytoplasm
Average fluorescence intensity (50 cells)
P = 8 × 10−14
m
LAMP1
n
LC3
o
WT mCAF
NUFIP1-KO mCAF
p
Autophagosome
Cell lysate
q
14838T
p-S6K
S6K
Actin
r
MIA Paca-2
s
Doxycycline
KRAS
t

Fig. 2 | Ribosomal RNA degradation is activated in CAFs under nutrient-limiting conditions. a–e, The 14837T cells, mCAFs, 8988T cells and hCAFs (**b** & **d**) cultured with or without glutamine for 48 h. RNA gel showed the degradation of RNA. The results represent $n = 3$ independent experiments. **f**,**g**, The 14837T cells (**f**), mCAFs (**f**) and NUFIP1-KO mCAFs (**g**) cultured with or without glutamine for 48 h. Western blotting was performed to determine r-protein levels. The results represent $n = 3$ independent experiments. **h**, The 14837T cells were infected with virus of flag-NUFIP1-WT and cultured without glutamine for 48 h. Then cells were immunoprecipitated using M2-flag beads. The co-precipitated RNAs were purified and analyzed by RT–qPCR. Data are shown as mean ± s.d. ($n = 3$ independent experiments). **i**,**j**, WT mCAFs, *NUFIP1*-KO mCAFs or autophagy-deficient mCAFs were cultured with or without glutamine for 48 h under actinomycin D (20 nM) treatment. RNA gel showed the degradation of RNA. The results represent $n = 3$ independent experiments. **k**,**l**, The 14837T cells and mCAFs cultured with or without glutamine for 48 h and then immunostained with anti-NUFIP1. Scale bars, 5 μm. The results represent $n = 3$ independent experiments. The fluorescence intensity of NUFIP1 in nucleus/cytoplasm was recorded (50 cells) (**l**). Data are shown as mean ± s.d. ($n = 50$). **m**,**n**, The mCAFs cultured without glutamine for 48 h and then immunostained with different antibodies. The results showed the co-localization of NUFIP1 with LAMP1 (**m**) or LC3 (**n**). Scale bars, 5 μm. The results represent $n = 3$ independent experiments. **o**,**p**, *STX17*-KO mCAFs and NUFIP1/STX17 double-KO mCAFs cultured without glutamine for 48 h. Autophagosomes were purified by the OptiPrep membrane flotation method. RNA gel showed the degradation of RNA (**o**). Western blotting was performed to determine LC3 and LAMP1 (**p**). The results represent $n = 3$ independent experiments. **q**,**r**, Mouse (**q**) or human (**r**) cells were cultured with or without glutamine for 48 h. Western blotting was then performed to determine p-S6K. The results represent $n = 3$ independent experiments. **s**,**t**, The 14837T cells cultured with or without doxycycline (1 μg ml^{-1}) (to turn on/off *iKRAS*) for 72 h. Then the cells were treated with no glutamine medium for 48 h. Western blotting was performed to determine p-S6K (**s**). Immunostaining was performed with the anti-NUFIP1 (**t**). Scale bars, 5 μm. The results represent $n = 3$ independent experiments. Statistical analysis was performed using ordinary one-way ANOVA with Tukey's multiple comparison test (**h**,**l**).

the CAFs and gradually depleted from CAF medium when incubated with PDAC cells (Fig. 3c–e). Therefore, a reasonable prediction would be that the nucleosides produced by CAFs could alleviate the nutrient stress promoted by glutamine deficiency in PDAC cells. To test this hypothesis, we incubated PDAC cells without glutamine in the absence or presence of exogenous nucleosides. We then found that supplementation of glutamine-free medium with nucleosides could also rescue growth in a manner similar to CAF CM (Fig. 3f–h). Moreover, nucleosides were able to restore the growth-promoting ability of CM from *NUFIP1*-KO CAFs (Fig. 3i–k). Collectively, these data indicated that CAF-secreted nucleosides have an impact on PDAC proliferation.

CAFs secrete nucleosides that promote PDAC metabolism. We next investigated how PDAC cells metabolize CAF-derived nucleosides. First, we noted that the level of nucleotides in PDAC was induced by the CM from WT CAFs (Fig. 4a and Extended Data Fig. 5a). Besides nucleotides, several metabolites were also increased by nucleosides and the CM from the WT CAFs, including glucose-6-P, fructose-6-P, pyruvate, citrate, succinate, fumarate and malate, indicating that glucose metabolic pathways were activated (Fig. 4b–d and Extended Data Fig. 5b,c). Furthermore, in comparison with cells treated with *NUFIP1*-KO CAF CM, the cells cultured in WT CAF CM demonstrated an increased oxygen consumption rate (OCR) (Fig. 4e). The cells treated with nucleosides also showed an increase in OCR compared with the untreated cells in glutamine-deprived conditions (Fig. 4f). We then performed [$^{13}C_5$]adenosine and [$^{13}C_5$] uridine tracing studies to assess how nucleosides were being used in PDAC metabolism. Treatment of cells with [$^{13}C_5$]adenosine/uridine led to an increase in the intracellular metabolites pool (Extended Data Fig. 5c,d). However, carbon from adenosine/uridine did not contribute to glycolytic intermediates or TCA intermediates (Extended Data Fig. 5d,e). These results suggest that nucleosides were not used in the glucose metabolic pathways as carbon sources.

In addition, we also detected whether nucleosides maintain glucose metabolism under low glucose conditions. As shown in Extended Data Fig. 6a, uridine and other nucleosides can support tumor growth under low glucose conditions. However, glycolysis and the TCA cycle were only slightly affected by nucleosides, whereas it seems that the pentose phosphate pathway was activated by uridine (Extended Data Fig. 6b). These data suggest that, in response to various nutritional stresses, nucleosides may sustain the cancer cells growth through different pathways.

Nucleosides promote glucose utilization in PDAC. Our data have shown that nucleosides cannot directly fuel PDAC metabolism. Consistent with the metabolite levels, our quantitative (q) PCR findings demonstrated a significant increase in the expression of genes involved in glucose consumption in PDAC cells cultured with WT CAF CM (Fig. 5a and Extended Data Fig. 7a–c). In addition, we found that the activation of this gene set in PDAC cells was induced by nucleoside treatment on glutamine starvation (Fig. 5b and Extended Data Fig. 7d,e). Among these genes, *slc2a1* is a well-known glucose transporter, therefore we hypothesized that the processes of glucose uptake may be involved in nucleoside-regulated PDAC metabolism. It has been reported that blockade of glutamine metabolism restricts glucose uptake and utilization[21]. Our data also showed that glucose uptake was repressed when PDAC cells were cultured in glutamine-free medium (Fig. 5c and Extended Data Fig. 7f). The CAF CM and nucleosides could both rescue the

Fig. 3 | CAFs secrete nucleosides dependent on NUFIP1. a,**b**, Relative content of nucleosides in cells (**a**) and medium (**b**). WT mCAFs and NUFIP1-KO mCAFs were cultured at the described glutamine concentrations for 48 h. Metabolic analysis of cells was performed by MS. Data are shown as mean ± s.d. ($n = 3$ biologically independent samples). **c**, Schematic of the metabolomic experiments depicted in **d** and **e**. **d**,**e**, WT mCAFs and NUFIP1-KO mCAFs cultured with glucose-free medium, which was supplemented with [$^{13}C_6$]glucose (25 mM) for 14 d. After that, the cells were cultured with or without glutamine for 48 h and the CM was collected. Isotope-labeled nucleosides were significantly elevated in WT mCAF CM, decreased in double CM (mCAF CM added to 14837T cells and then collected) (**d**) and elevated intracellularly in 14837T cells treated with mCAF CM (**e**). Data are shown as mean ± s.d. ($n = 3$ biologically independent samples). Pairwise comparisons were conducted using two-tailed, unpaired Student's *t*-tests. **f**–**h**, The 14837T, 14838T (**f**), 8988T, 8988S (**g**), hPDAC-1 and hPDAC-2 (**h**) cells were cultured in no glutamine medium with or without uridine (U, 0.5 mM), inosine (I, 0.5 mM), adenosine (A, 0.5 mM), guanosine (G, 0.5 mM) and cytidine (C, 0.5 mM) for 48 h. The cells were counted to calculate the cell proliferation. Data are shown as mean ± s.d. ($n = 4$ independent samples). **i**–**k**, The 14837T (**i**), 8988T (**j**), hPDAC-1 and hPDAC-2 (**k**) cells were cultured in CM (no glutamine) from WT CAFs and NUFIP1-KO CAFs with or without U, I, A, G and C (0.5 mM each) for 48 h. The cells were counted to calculate the cell proliferation. Data are shown as mean ± s.d. ($n = 4$ independent samples). Statistical analysis was performed using ordinary one-way ANOVA with Tukey's multiple comparison test (**a**,**b**,**f**–**k**).

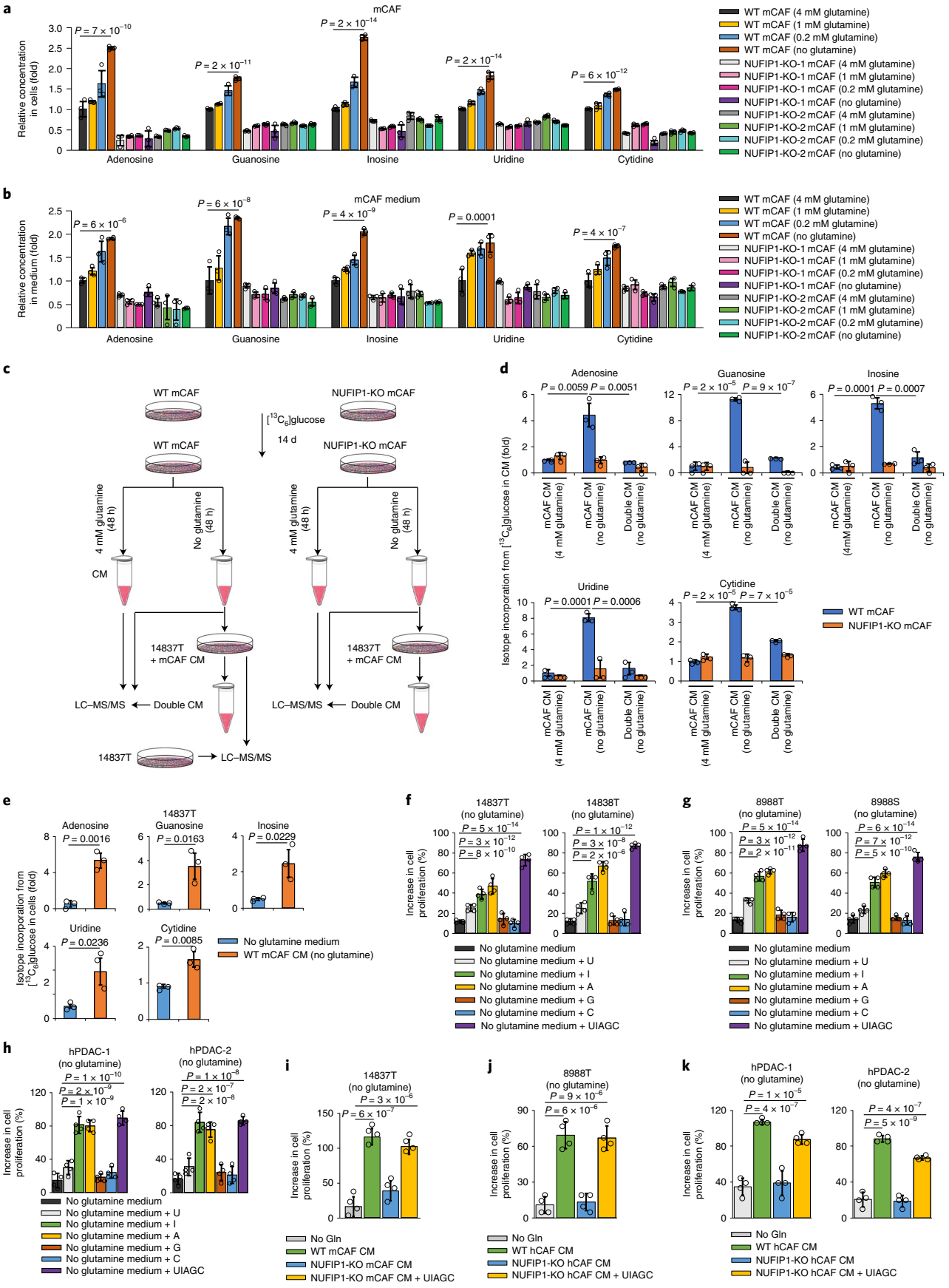
a
mCAF
Relative concentration in cells (fold)
P = 7 × 10−10
P = 2 × 10−11
P = 2 × 10−14
P = 2 × 10−14
P = 6 × 10−12
Adenosine
Guanosine
Inosine
Uridine
Cytidine
WT mCAF (4 mM glutamine)
WT mCAF (1 mM glutamine)
WT mCAF (0.2 mM glutamine)
WT mCAF (no glutamine)
NUFIP1-KO-1 mCAF (4 mM glutamine)
NUFIP1-KO-1 mCAF (1 mM glutamine)
NUFIP1-KO-1 mCAF (0.2 mM glutamine)
NUFIP1-KO-1 mCAF (no glutamine)
NUFIP1-KO-2 mCAF (4 mM glutamine)
NUFIP1-KO-2 mCAF (1 mM glutamine)
NUFIP1-KO-2 mCAF (0.2 mM glutamine)
NUFIP1-KO-2 mCAF (no glutamine)
b
mCAF medium
Relative concentration in medium (fold)
P = 6 × 10−6
P = 6 × 10−8
P = 4 × 10−9
P = 0.0001
P = 4 × 10−7
Adenosine
Guanosine
Inosine
Uridine
Cytidine
c
WT mCAF
NUFIP1-KO mCAF
[13C6]glucose
14 d
4 mM glutamine (48 h)
No glutamine (48 h)
CM
14837T + mCAF CM
LC–MS/MS
Double CM
14837T
d
Adenosine
P = 0.0059 P = 0.0051
Guanosine
P = 2 × 10−5 P = 9 × 10−7
Inosine
P = 0.0001 P = 0.0007
Uridine
P = 0.0001 P = 0.0006
Cytidine
P = 2 × 10−5 P = 7 × 10−5
Isotope incorporation from [13C6]glucose in CM (fold)
mCAF CM (4 mM glutamine)
mCAF CM (no glutamine)
Double CM (no glutamine)
WT mCAF
NUFIP1-KO mCAF
e
Adenosine
P = 0.0016
14837T Guanosine
P = 0.0163
Inosine
P = 0.0229
Uridine
P = 0.0236
Cytidine
P = 0.0085
Isotope incorporation from [13C6]glucose in cells (fold)
No glutamine medium
WT mCAF CM (no glutamine)
f
14837T (no glutamine)
14838T (no glutamine)
Increase in cell proliferation (%)
P = 5 × 10−14
P = 3 × 10−12
P = 8 × 10−10
P = 1 × 10−12
P = 3 × 10−8
P = 2 × 10−6
No glutamine medium
No glutamine medium + U
No glutamine medium + I
No glutamine medium + A
No glutamine medium + G
No glutamine medium + C
No glutamine medium + UIAGC
g
8988T (no glutamine)
8988S (no glutamine)
P = 5 × 10−14
P = 3 × 10−12
P = 2 × 10−11
P = 6 × 10−14
P = 7 × 10−12
P = 5 × 10−10
h
hPDAC-1 (no glutamine)
hPDAC-2 (no glutamine)
P = 1 × 10−10
P = 2 × 10−9
P = 1 × 10−9
P = 1 × 10−8
P = 2 × 10−7
P = 2 × 10−8
i
14837T (no glutamine)
P = 6 × 10−7
No Gln
WT mCAF CM
NUFIP1-KO mCAF CM
NUFIP1-KO mCAF CM + UIAGC
j
8988T (no glutamine)
P = 9 × 10−6
P = 6 × 10−6
No Gln
WT hCAF CM
NUFIP1-KO hCAF CM
NUFIP1-KO hCAF CM + UIAGC
k
hPDAC-1 (no glutamine)
P = 1 × 10−5
P = 4 × 10−7
hPDAC-2 (no glutamine)
P = 4 × 10−7
P = 5 × 10−9
No Gln
WT hCAF CM
NUFIP1-KO hCAF CM
NUFIP1-KO hCAF CM + UIAGC

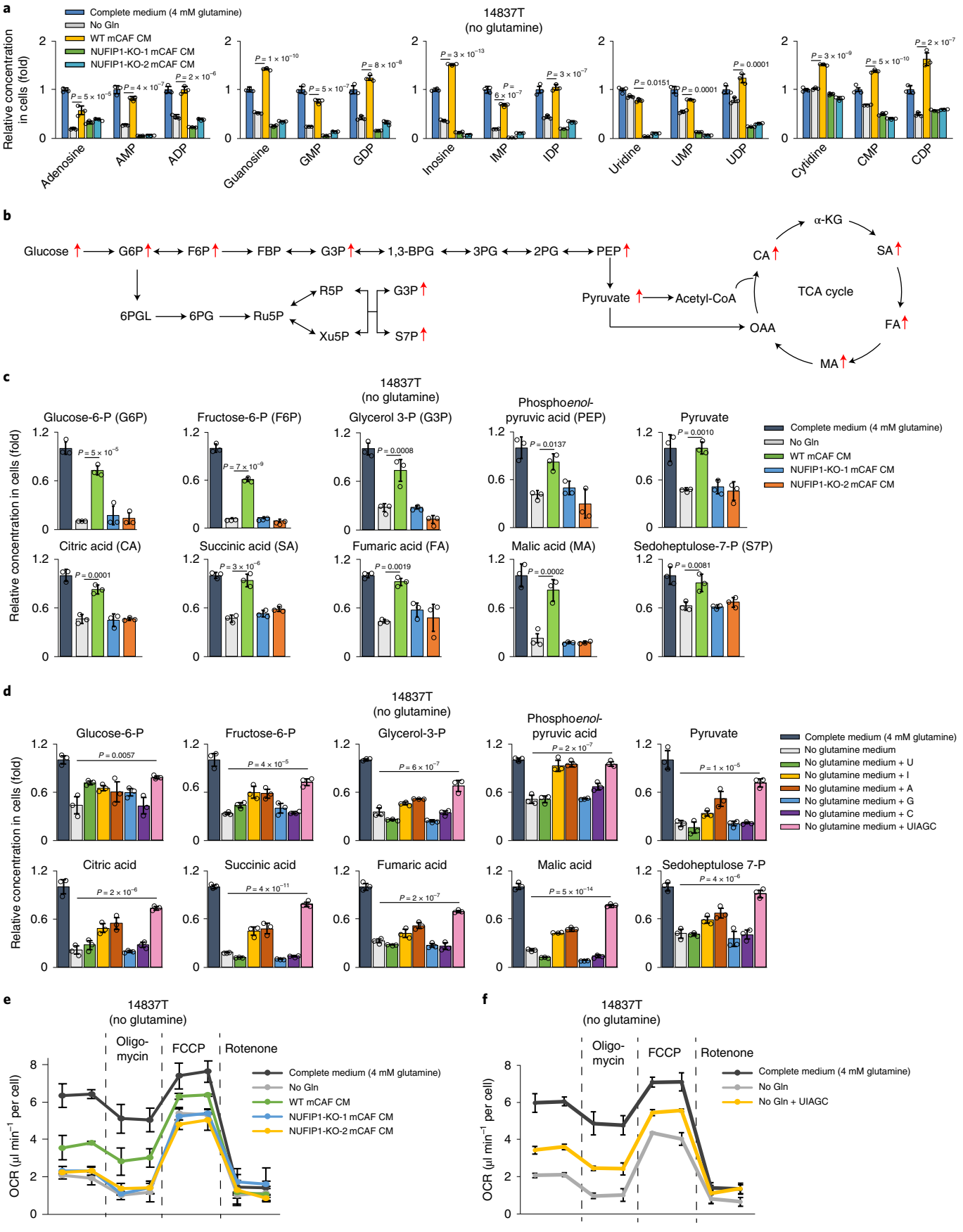
a
Complete medium (4 mM glutamine)
No Gln
WT mCAF CM
NUFIP1-KO-1 mCAF CM
NUFIP1-KO-2 mCAF CM
14837T (no glutamine)
Relative concentration in cells (fold)
Adenosine
AMP
ADP
Guanosine
GMP
GDP
Inosine
IMP
IDP
Uridine
UMP
UDP
Cytidine
CMP
CDP
b
Glucose
G6P
F6P
FBP
G3P
1,3-BPG
3PG
2PG
PEP
6PGL
6PG
Ru5P
R5P
Xu5P
S7P
Pyruvate
Acetyl-CoA
CA
α-KG
SA
FA
MA
OAA
TCA cycle
c
Glucose-6-P (G6P)
Fructose-6-P (F6P)
Glycerol 3-P (G3P)
Phosphoenol-pyruvic acid (PEP)
Pyruvate
Citric acid (CA)
Succinic acid (SA)
Fumaric acid (FA)
Malic acid (MA)
Sedoheptulose-7-P (S7P)
d
Glucose-6-P
Fructose-6-P
Glycerol-3-P
Phosphoenol-pyruvic acid
Pyruvate
Citric acid
Succinic acid
Fumaric acid
Malic acid
Sedoheptulose 7-P
No glutamine medium
No glutamine medium + U
No glutamine medium + I
No glutamine medium + A
No glutamine medium + G
No glutamine medium + C
No glutamine medium + UIAGC
e
Oligo-mycin
FCCP
Rotenone
OCR (μl min−1 per cell)
f
No Gln + UIAGC

Fig. 4 | CAFs secrete nucleosides that promote pancreatic cancer metabolism. a, The 14837T cells cultured in complete medium (4 mM glutamine) or CM (no glutamine) from different cell lines for 48 h. Nucleosides and nucleotides in the cells were analyzed by MS. Data are shown as mean ± s.d. ($n = 3$ biologically independent samples). **b**, Summary of altered metabolites in the glycolysis pathway and TCA cycle. An increase in metabolite levels is indicated with a red upward arrow. 1,3-BPG, 1,3-bisphosphoglyceric acid; 2PG, 2-phosphoglycerate; 3PG, 3-phosphoglycerate; 6PG, 6-phosphogluconic acid; 6PGL, 6-phosphogluconolactonase; FBP, fructose-1,6-bisphosphate; OAA, oxaloacetate; R5P, ribose-5-phosphate; Ru5P, ribulose-5-phosphate; Xu5P, xylulose 5-phosphate. **c**, The 14837T cells were cultured in complete medium (4 mM glutamine), no glutamine medium or CM (no glutamine) from WT mCAFs and NUFIP1-KO mCAFs for 48 h. Metabolic analysis of cells was performed by MS. Data are shown as mean ± s.d. ($n = 3$ biologically independent samples). **d**, The 14837T cells cultured in complete medium (4 mM glutamine), no glutamine medium with or without U (0.5 mM), I (0.5 mM), A (0.5 mM), G (0.5 mM) and C (0.5 mM) for 48 h. Metabolic analysis of cells was performed by MS. Data are shown as mean ± s.d. ($n = 3$ biologically independent samples). **e**,**f**, The 14837T cells cultured with CM (no glutamine) from WT mCAFs, *NUFIP1*-KO-1 or *NUFIP1*-KO-2 mCAFs (**e**) or U, I, A, G and C (0.5 mM each) (**f**) for 48 h. After that, the cells were exposed to oligomycin (2 μM), FCCP (0.5 μM) and rotenone (1 μM) to measure the OCR and each treatment was measured at 30 min and 60 min, respectively. Data are shown as mean ± s.d. ($n = 3$ biologically independent samples). Statistical analysis was performed using ordinary one-way ANOVA with Tukey's multiple comparison test (**a**,**c**,**d**).

glucose uptake activity of PDAC (Fig. 5c and Extended Data Fig. 7f). To confirm whether glucose utilization was changed by CAFs, we quantified the abundance of specific isotopologs generated via glycolysis and TCA metabolism in PDAC cells cultured with [$^{13}C_6$]glucose. As depicted in Fig. 5d,e, the abundance of M6-G6P, M6-F6P, M3-3PG, M6-pyruvate, M2/M4/M5-citrate, M2/M4-αKG, M2/M3-succinate and M2/M3-malate was significantly increased by nucleosides and CAF CM compared with control cells when both were cultured without glutamine.

To further confirm the role of glucose uptake, we cultured CAFs under low glucose (5 mM glucose). As shown in Fig. 5f,g and Extended Data Fig. 7g,h, the tumor-promoting activity of nucleosides and CM from CAFs was impaired under low glucose conditions. Moreover, we also used a doxycycline-inducible short hairpin (sh)RNA to downregulate *slc2a1*'s expression (Fig. 5h). *Slc2a1* knockdown experiments also suggested the importance of glucose uptake for the growth-promoting effect of CM from CAFs and nucleosides (Fig. 5i,j).

CAFs activate glucose consumption in PDAC dependent on MYC. Gene-set enrichment analysis (GSEA) of a transcriptomic profiling of 14837T cells revealed that, in the absence of glutamine, 14837T cells cultured with WT CAF CM displayed enrichment of a gene expression signature that corresponds to the 'MYC-targets' category (Fig. 6a). *MYC* is an important transcriptional regulator of glucose metabolism[22]. We observed that WT CAF CM induced a higher level of *MYC* under glutamine-deprived conditions (Fig. 6b). In addition, the equilibrative nucleoside transporter (ENT) inhibitor dipyridamole, but not inhibitors of adenosine-producing ecto-enzyme or adenosine receptor, impaired the *MYC*-dependent transcriptional activation by CAF CM (Fig. 6c–e and Extended Data Fig. 8a–e), indicating that *MYC* activation in tumors is probably due to the direct transfer of nucleosides.

To determine whether the increased glucose utilization induced by CAFs is *MYC* dependent, we stably knocked down *MYC* in PDAC cells. As shown in Fig. 6f–i and Extended Data Fig. 8f–j, CAF CM or nucleosides that induced glucose consumption gene expression under glutamine-deprived conditions displayed a dependence on *MYC*. Knocking down *MYC* also inhibited the OCR and glucose consumption in WT CAF CM-treated PDAC cells (Fig. 7a–c). Similarly, nucleosides activated glucose uptake and utilization was also dependent on *MYC* (Fig. 7a–c). As *MYC* is also a master regulator of nucleotide synthesis genes[22], we tested the expression of purine and pyrimidine synthesis genes. As shown in Extended Data Fig. 9a,b, we found that *PHGDH, PSPH* and *SHMT2* expression levels could be induced by WT CAF CM, but not by *NUFIP1*-KO CAF CM. Furthermore, CAF CM induced expression of these genes under glutamine-deprived conditions displaying dependence on *MYC* (Extended Data Fig. 9c). Collectively, these data indicate that *MYC* is required for CAF CM-induced expression of genes involved in the synthesis of serine and glycine, but not for genes that directly regulate salvage and de novo nucleotide synthesis pathways.

Cellular adenosine controls the translation of endogenous *MYC* via the 3′-UTR of the *MYC* mRNA[23]. To test whether CAF CM could also regulate *MYC* translation via the 3′-UTR, we expressed *MYC* from constructs that encompass either the coding sequence or the coding sequence with 3′-UTR in *MYC* knockdown cells. As shown in Fig. 6d,e, only inclusion of the 3′-UTR led to the induction of MYC protein by CAF CM or nucleosides. Moreover, polysome profiling was also used to infer the translational status of *MYC* mRNA. We found that CAF CM or nucleosides induced endogenous *MYC* mRNA to shift toward heavier polysome fractions (Fig. 6f), suggesting that *MYC* translation is increased. To confirm that the increased *MYC* translation was related to tumor growth, we next tested the

Fig. 5 | Nucleosides promote energy metabolism in PDAC by increasing glucose utilization. a, The 14837T cells cultured in complete medium or CM (no glutamine) from different cell lines for 48 h. RNA was then extracted and analyzed with RT-PCR. Data are shown as mean ± s.d. ($n = 3$ independent experiments). **b**, The 14837T cells were cultured in complete medium or no glutamine medium with or without U, I, A, G and C (0.5 mM each) for 48 h. RNA was then extracted and analyzed with RT-PCR. Data are shown as mean ± s.d. ($n = 3$ independent experiments). **c**, The 14837T cells cultured with complete medium, no glutamine medium with U, I, A, G and C (0.5 mM each) or CM (no glutamine) from different cell lines for 48 h. The relative value of glucose uptake was then measured. Data are shown as mean ± s.d. ($n = 3$ independent samples). **d**, Metabolic map depicting glycolysis and TCA cycle downstream of a [$^{13}C_6$]glucose tracer. **e**, The 14837T cells cultured with complete medium, no glutamine medium with or without U, I, A, G and C or CM (no glutamine) with [$^{13}C_6$]glucose (25 mM) for 48 h. Glucose-derived, carbon-labeling patterns of metabolites demonstrated substantial label incorporation into the glucose metabolites. Data are shown as mean ± s.d. ($n = 3$ independent samples). **f**, The 14837T cells cultured in different medium (no glutamine, 25 mM or 5 mM glucose) with or without U, I, A, G and C (0.5 mM each) for 48 h. The cells were counted to calculate the cell proliferation. Data are shown as mean ± s.d. ($n = 4$ independent samples). **g**, The 14837T cells cultured in CM (no glutamine, 25 mM or 5 mM glucose) from different cell lines with for 48 h. The cells were counted to calculate the cell proliferation. Data are shown as mean ± s.d. ($n = 4$ independent samples). **h**, The 8988T cells treated with doxycycline at different concentrations to induce *slc2a1* knockdown. The results represent $n = 3$ independent experiments. **i**, The 8988T (WT) and 8988T (*slc2a1* knockdown) cells treated with CM (no glutamine) from 8988T cells and hCAFs and then counted. Data are shown as mean ± s.d. ($n = 4$ independent samples). **j**, The 8988T cells treated with or without U, I, A, G and C and then counted. Data are shown as mean ± s.d. ($n = 4$ independent samples). Statistical analysis was performed using ordinary one-way ANOVA with Tukey's multiple comparison test (**a**–**c**,**e**–**g**,**i**,**j**).

effect of CAF CM on *MYC*-knockdown or *MYC*-3′-UTR-expressing cell lines. We observed that the expression of *MYC*-3′-UTR mediated the growth-promoting effect of CAF CM or nucleosides (Fig. 6g and Extended Data Fig. 9d–f), demonstrating a critical role for *MYC*-3′-UTR in maintaining pancreatic tumor cell survival.

In vivo effect of NUFIP1 in PDAC. As further confirmation of the importance of this pathway in PDAC, we examined the efficacy of autophagy inhibitor chloroquine (CHQ) with GLS inhibitor in an orthotopic model of PDAC. Strikingly, combination therapy resulted in significant tumor growth inhibition (Fig. 8a).

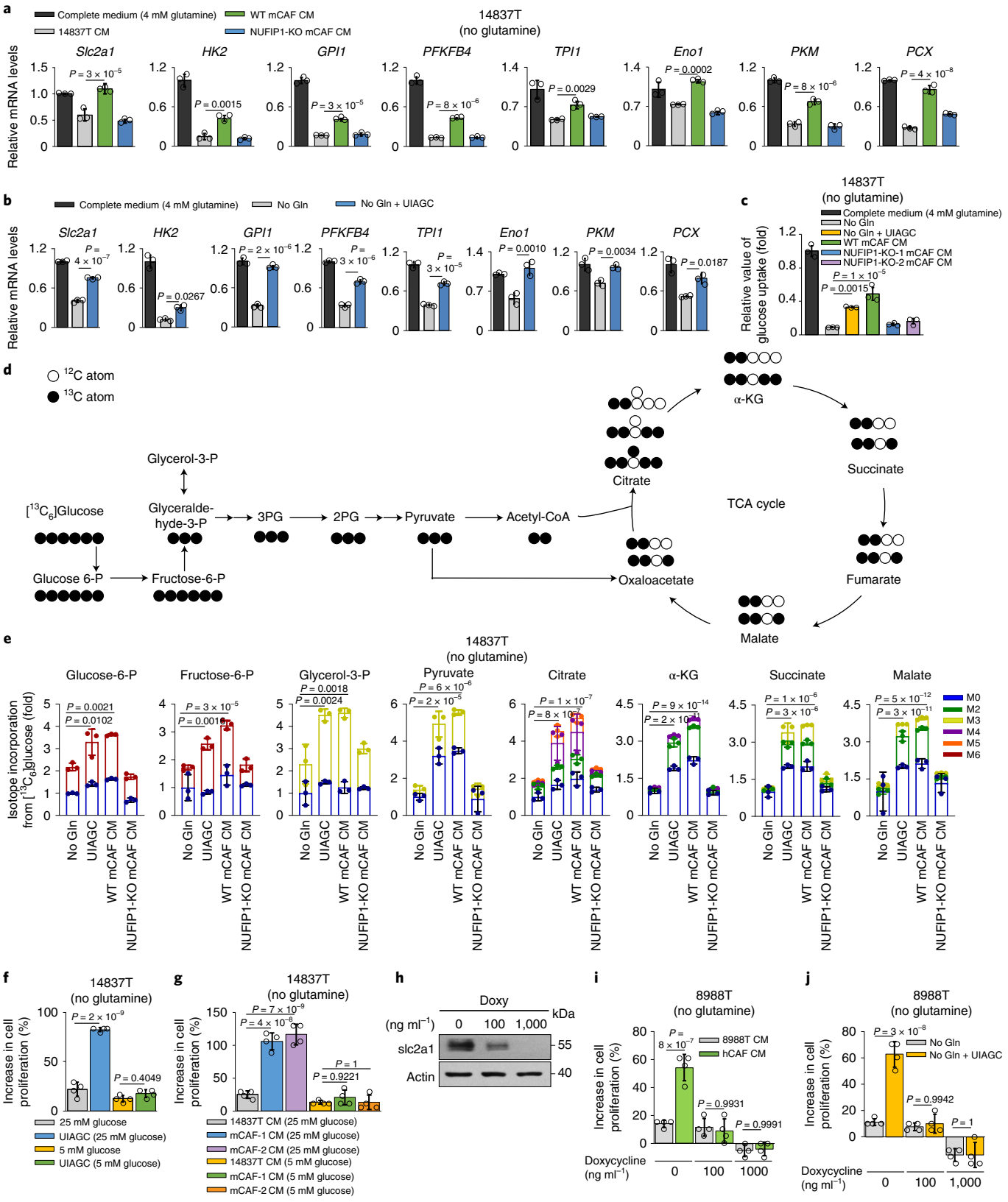

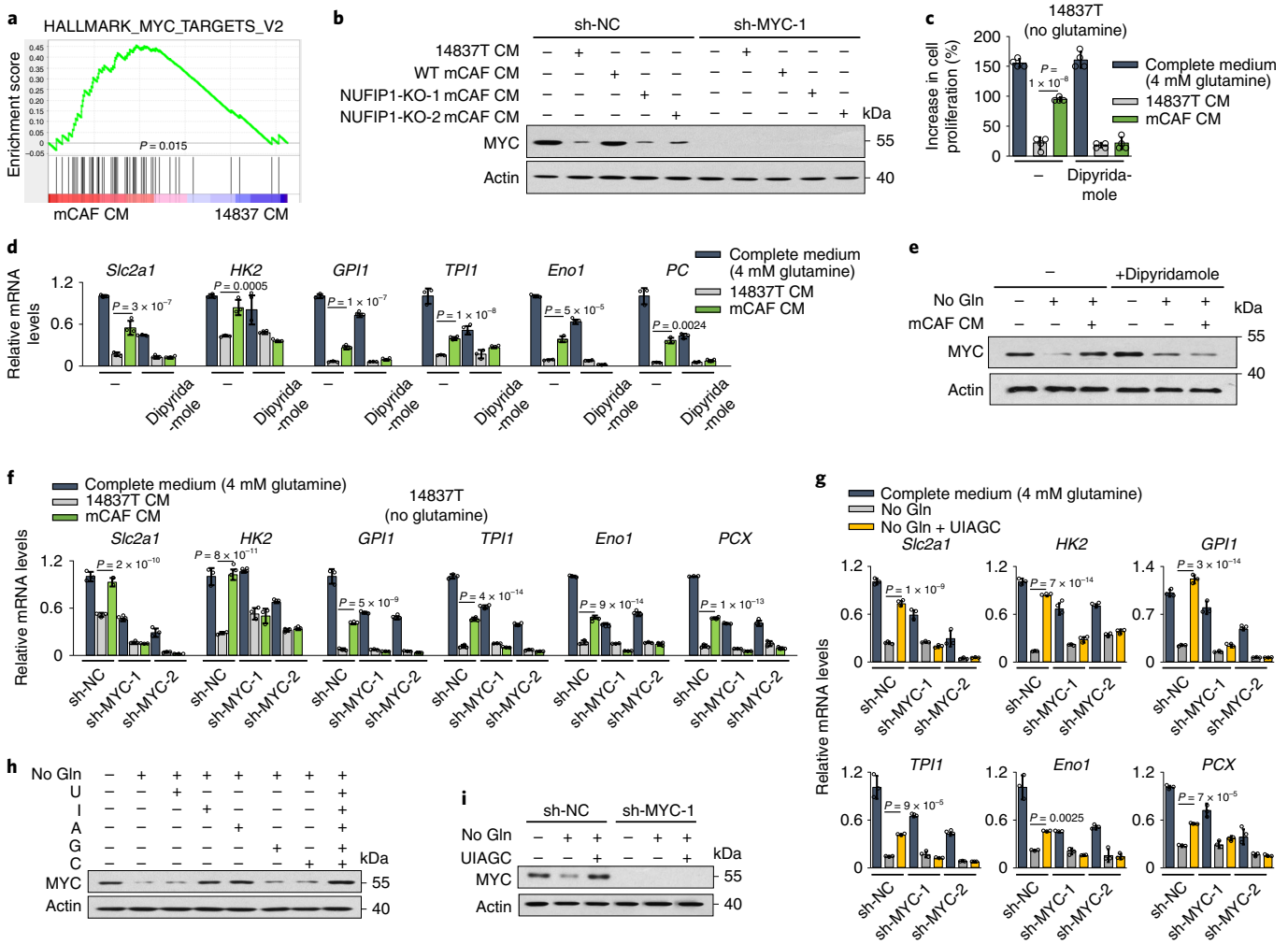

Fig. 6 | CAF CM induced glucose consumption gene expression. a, GSEA plot of enrichment in 'HALLMARK_MYC_TARGETS_V2'. The 14837T cells were cultured in CM (no glutamine) from 14837T cells or mCAFs. The *P* value was automatically determined by GSEA v.3.0. **b**, The 14837T (WT) and 14837T (*MYC* knockdown) cells cultured in complete medium (4 mM glutamine) or CM (no glutamine) from 14837T cells or mCAFs for 48 h. Western blotting was performed to determine MYC protein levels. The results represent $n = 3$ independent experiments. **c**–**e**, The 14837T cells treated with ENT inhibitor dipyridamole (10 μM) and cultured in complete medium (4 mM glutamine) or CM (no glutamine) from 14837T cells or mCAFs for 48 h. The cells were counted to calculate the cell proliferation (**c**). Data are shown as mean ± s.d. ($n = 4$ independent samples). RNA was then extracted and analyzed with RT-PCR (**d**). Data are shown as mean ± s.d. ($n = 3$ independent experiments). Western blotting was performed to determine MYC protein levels (**e**). The result represent $n = 3$ independent experiments. **f**, The 14837T (WT) and 14837T (*MYC* knockdown) cells cultured in complete medium (4 mM glutamine) or CM (no glutamine) from 14837T cells or mCAFs for 48 h. RNA was then extracted and analyzed with RT-PCR. Data are shown as mean ± s.d. ($n = 3$ independent experiments). **g**, The 14837T (WT) and 14837T (*MYC* knockdown) cells cultured in complete medium (4 mM glutamine) or no glutamine medium with or without U, I, A, G and C (0.5 mM each) for 48 h. RNA was then extracted and analyzed with RT-PCR. Data are shown as mean ± s.d. ($n = 3$ independent experiments). **h**, The 14837T cells cultured in complete medium (4 mM glutamine) or no glutamine medium with or without U, I, A, G and C (0.5 mM each) for 48 h. Western blotting was performed to determine MYC protein levels. The results represent $n = 3$ independent experiments. **i**, The 14837T (WT) and 14837T (*MYC* knockdown) cells cultured in complete medium (4 mM glutamine) or no glutamine medium with or without U, I, A, G and C (0.5 mM each) for 48 h. Western blotting was performed to determine MYC protein levels. The results represent $n = 3$ independent experiments. Statistical analysis was performed using ordinary one-way ANOVA with Tukey's multiple comparisons test (**c**,**d**,**f**,**g**).

As stromal autophagy promotes tumor desmoplasia[24], we generated a fibroblast-specific conditional *NUFIP1* KO model by crossing *NUFIP1*$^{fl/fl}$ mice with *FSP1-Cre* mice to test whether NUFIP1 contributes to desmoplasia (Fig. 8b). Then we implanted 14837T cells into the pancreas of *FSP-Cre;NUFIP1*$^{fl/fl}$ mice and *FSP-Cre;Atg5*$^{fl/fl}$ mice and performed Masson's Trichrome staining on orthotopic tumors. As shown in Extended Data Fig. 10a–d, there was less collagen content in *FSP-Cre;Atg5*$^{fl/fl}$ mice, but not in *FSP-Cre;NUFIP1*$^{fl/fl}$ mice, indicating that NUFIP1 does not affect the desmoplastic response in PDAC. To further validate the importance of CAFs, we tested the growth of 14837T cells in *FSP-Cre;NUFIP1*$^{fl/fl}$ mice and *FSP-Cre;Atg5*$^{fl/fl}$ mice. In an orthotopic model of PDAC, tumors were significantly smaller when grown in *FSP-Cre;NUFIP1*$^{fl/fl}$ mice and *FSP-Cre;Atg5*$^{fl/fl}$ mice compared with WT mice (Fig. 8c and Extended Data Fig. 10e). In addition, Ki67-positive cell populations were substantially reduced in *FSP-Cre;NUFIP1*$^{fl/fl}$ mice and *FSP-Cre;Atg5*$^{fl/fl}$ mice compared with WT, demonstrating that NUFIP1 in the CAFs promoted PDAC growth in vivo (Fig. 8d,e). Moreover, consistent with the in vitro proliferation data, tumor growth was significantly increased when co-injected with WT CAFs, and this increase was significantly attenuated when PDAC cells were co-injected with NUFIP1^{W35A}-expressing CAFs or *NUFIP1*-KO CAFs (Fig. 8f–h).

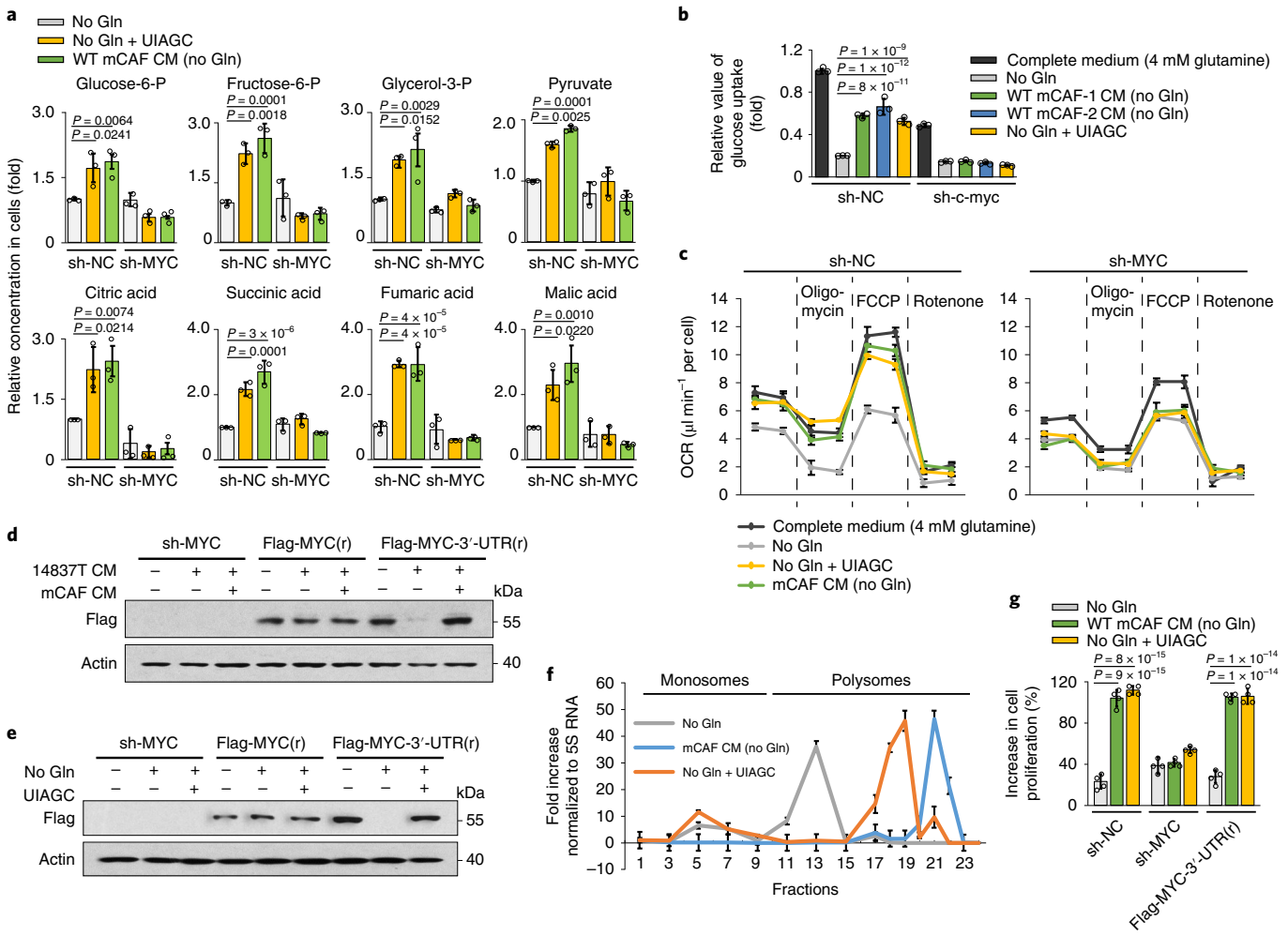

Fig. 7 | CAFs activate glucose consumption in PDAC dependent on MYC. a,b, The 14837T (WT) and 14837T (*MYC* knockdown) cells cultured in no glutamine medium with or without U, I, A, G and C (0.5 mM each) or CM (no glutamine) from mCAFs for 48 h. Metabolic analysis of cells was performed by MS (**a**). The relative value of glucose uptake was measured by the Glucose Uptake-Glo Assay kit (**b**). Data are shown as mean ± s.d. ($n = 3$ biologically independent samples). Statistical analysis was performed using ordinary one-way ANOVA with Tukey's multiple comparisons test. **c**, The 14837T (WT) and 14837T (*MYC* knockdown) cells cultured in 96-well plates with complete medium (4 mM glutamine), no glutamine medium with U, I, A, G and C (0.5 mM each) or CM (no glutamine) from 14837T cells or mCAFs for 48 h. After that, the cells were exposed to oligomycin (2 μM), FCCP (0.5 μM) and rotenone (1 μM) to measure the OCR and each treatment was measured at 30 min and 60 min, respectively. Data are shown as mean ± s.d. ($n = 3$ biologically independent samples). **d**,**e**, The shRNA-resistant flag-*MYC*(r) and flag-*MYC*-3′-UTR(r) were overexpressed in *MYC* knockdown 14837T cells. The cells were cultured with CM from mCAFs (**d**) or U, I, A, G and C (**e**) for 48 h. Western blotting was performed to determine flag-*MYC* levels. The results represent $n = 3$ independent experiments. **f**, The 14837T cells cultured in no glutamine medium with or without U, I, A, G and C (0.5 mM each) or CM (no glutamine) from mCAFs for 48 h. Polysomes were fractionated on sucrose density gradients. The mRNA levels were measured by qPCR and normalized to 5S rRNA level. Data are shown as mean ± s.d. ($n = 3$ independent experiments). **g**, Cell proliferation of 14837T cells treated with complete medium (4 mM glutamine) or CM (no glutamine) from 14837T cells or mCAFs. Data are shown as mean ± s.d. ($n = 4$ independent samples). Statistical analysis was performed using ordinary one-way ANOVA with Tukey's multiple comparison test.

We next explored whether the effects of *MYC* activation on PDAC cells was dependent on CAF-secreted nucleosides. TIF was isolated from orthotopic mouse models and the concentration of nucleosides in the TIF was detected. As shown in Fig. 8i, the level of nucleotides in TIF was decreased in *FSP-Cre*;*NUFIP1*$^{fl/fl}$ mice compared with WT mice, indicating that NUFIP1 in CAFs plays important roles in maintaining the level of nucleosides in the stroma. Next, we analyzed the expression of *MYC* by immunohistochemistry (IHC) staining of tumor tissues. We implanted PDAC cells with WT CAFs, NUFIP1^{W35A}-expressing CAFs and *NUFIP1*-KO CAFs into the pancreas of mice. *MYC* signal was significantly attenuated in CK19^{+} tumor cells when PDAC cells were co-injected with NUFIP1^{W35A}-expressing CAFs or *NUFIP1*-KO CAFs (Fig. 8j). Moreover, the expression of *MYC* was clearly repressed in the tumor tissues in the *FSP-Cre*;*NUFIP1*$^{fl/fl}$ orthotopic model compared with that in WT mice (Fig. 8k). These results suggest that reduced nucleoside levels in the stroma results in *MYC* inactivation in PDAC cells. In addition, the tumor growth of orthotopic models in WT mice showed a dependence on *MYC* (Fig. 8l), whereas the dependence was impaired in *FSP-Cre*;*NUFIP1*$^{fl/fl}$ mice, further indicating the role of *MYC* activation in the tumor's response to CAF-secreted nucleosides.

To investigate the expression profiles of NUFIP1 in the PDAC stroma, we conducted IHC staining for NUFIP1 on a PDAC tissue microarray (TMA) containing 80 PDAC specimens. A subset of patients had high stromal expression of NUFIP1 observed

in 39 (49%) of the 80 PDAC cases. We found that high stromal NUFIP1 protein expression in the stroma was associated with significantly worse overall survival (Fig. 8m,n). By contrast, expression of NUFIP1 in the tumor compartment did not predict survival (Extended Data Fig. 10f,g), which highlights the importance of stromal ribophagy in PDAC.

Discussion

Glucose and glutamine are two of the most abundant nutrients consumed by neoplastic cells. To adapt to the nutrition-deprived microenvironment, CAF metabolism is always hijacked to meet the metabolic needs of tumor cells[25]. For instance, CAF-secreted glutamine maintains the growth of ovarian cancer cells under Gln starvation[26]. Glutamine secreted by prostate CAFs induces mitochondrial bioenergetics and prostate cancer neuroendocrine differentiation and tumor growth[27]. The pancreatic stroma produces alanine, which acts as an alternative carbon source to fuel the TCA cycle in PDAC[7]. CAF-secreted branched-chain α-ketoacid (BCKA) fuels the BCKA demand for PDAC[28]. In our study, we found that autophagy in CAFs generates nucleosides, which activate the *MYC* pathway to induce glucose consumption.

About 80% RNA was distributed as rRNA[29]. It is reasonable that degradation of rRNA yields massive nucleosides. Our results indicated that autophagy is required for rRNA degradation on glutamine starvation (Fig. 2e). The CM from *Atg3*-KO CAFs and *NUFIP1*-KO CAFs has effects on nucleoside secretion, *MYC* activation and tumor cell glycolytic metabolism (Extended Data Figs. 4e,f, 5c and 8j). However we did not observe obvious degradation of r-protein. A recent study using quantitative proteomics also showed that r-protein turnover occurs through nonautophagic pathways[17]. Therefore, we speculated that r-protein and rRNA disassociate from each other on glutamine starvation. R-proteins are degraded by proteasome, whereas rRNA translocated into autophagosome for subsequent degradation and translocation is mediated by NUFIP1. Indeed, the autophagosome accumulation of rRNA was fully suppressed by NUFIP1 impairment (Fig. 2o,p), indicating that NUFIP1 plays a critical role in translocation of rRNA to the autophagosome. In addition, we also tested the RNA-binding activity of NUFIP1^{W35A}, a mutant showing defects on interacting with LC3 (ref. [13]) (Extended Data Fig. 1f). As shown in Extended Data Fig. 2l, both WT and mutant NUFIP1 interact with rRNA. However, the nucleoside secretion level of NUFIP1^{W35A}-expressing CAFs was lower than that of NUFIP1^{WT}-expressing CAFs (Extended Data Fig. 4c,d), further suggesting that NUFIP1-mediated translocation of rRNA to autophagosome plays an important role in NUFIP-dependent nucleoside release from CAFs.

Nucleoside supplementation improved the proliferation of cancer cells under glucose or glutamine starvation[30–32]. There is no significant difference in amino acid secretion activity between WT CAFs and *NUFIP1*-KO CAFs (Extended Data Fig. 4g), indicating the role of nucleosides in tumor growth. Moreover, our data showed that, in addition to fueling nucleotide biosynthesis, nucleosides can also support glycolysis/TCA cycle and contribute to the adaptation of cells to glutamine starvation by activating *MYC*. We tested the effects of individual nucleosides and found that both inosine and adenosine can rescue cell proliferation in the absence of glutamine (Fig. 3f–h). In addition, MYC protein levels can be induced by inosine and adenosine, but not other nucleosides (Fig. 6b). Knocking down *MYC* in tumors significantly repressed the ability of inosine/adenosine to rescue tumor growth (Extended Data Fig. 9d), indicating that the rescue effect of inosine/adenosine is dependent on *MYC* activation.

The oncogene *MYC* is activated in many PDAC cases and is a master regulator of carbohydrate metabolism[33]. The growth-promoting effect of CAFs or nucleosides was impaired in *MYC*-downregulated PDAC (Fig. 7g and Extended Data Fig. 9e,f), indicating that the effect is *MYC* dependent. Endogenous *MYC* plays important roles in maintaining basal rates of glycolysis and oxidative phosphorylation in neoplastic cells[34]. Moreover, it is both necessary and potentially sufficient for the glutaminolytic metabolism and glutamine addiction in tumors[35]. However, on glutamine deprivation, colon cancer cells that express high levels of *MYC* are not glutamine addicted but undergo cell cycle arrest, because glutamine deprivation suppresses *MYC* levels[23]. We also found that glutamine starvation did not dramatically induce cell death, but only reduced cell growth in several PDAC cell lines (Extended Data Fig. 1a). In addition, the PDAC growth was promoted by CAF CM, even though MYC protein levels were also increased by CAFs in the absence of glutamine. We explored why tumor cells with high levels of *MYC* are not glutamine addicted. *MYC* diverts glucose-derived pyruvate away from mitochondrial metabolism by upregulating lactate dehydrogenase A (LDHA), leading to enhanced cellular dependence on glutamine[35]. Then we tested LDHA mRNA levels and found that they were not induced by CAF CM (Extended Data Fig. 9b). In contrast, another *MYC* target PC (pyruvate carboxylase)[36], an enzyme that catalyzes the ATP-dependent carboxylation of pyruvate to oxaloacetate, was increased after treatment with CAF CM (Fig. 5a). This indicated that, on glutamine starvation, CAF CM enhanced the metabolic flux through PC and promoted the synthesis of oxaloacetate and acetyl-CoA, both of which will generate citrate and subsequently 2-oxoglutarate. Several studies have shown that apoptosis induced by glutamine deprivation could be inhibited by providing the cell-permeable TCA substrate 2-oxoglutarate or oxaloacetate[35,37]. Therefore, we speculated that compensating for the lack of glutamine-derived 2-oxoglutarate by the *MYC*–PC pathway mediated the protection effect of CAFs under glutamine-deprivation conditions.

In summary, the findings we present in the present report provide mechanistic insights into the metabolic connection between PDAC and the tumor stroma. Our findings indicate that CAFs

Fig. 8 | In vivo effect of NUFIP1 in PDAC. a, CHQ and 968 injected intraperitoneally into orthotopic models of PDAC from day 5. After 14 d, the tumors were weighed. Data are shown as mean ± s.d. ($n = 6$ mice). **b**, Orthotopic PDAC models in WT and *FSP-Cre;NUFIP1*$^{fl/fl}$ mice. The tumors were analyzed by NUFIP1 and α-SMA IHC staining. Scale bars, 30 μm. The results represent images from three independent mice. **c**–**e**, Orthotopic PDAC models in WT, *FSP-Cre;ATG5*$^{fl/fl}$ and *FSP-Cre;NUFIP1*$^{fl/fl}$ mice. The tumors were weighed ($n = 6$ mice) (**c**) and analyzed by Ki67 IHC staining ($n = 10$ views) (**d**,**e**). Scale bars, 20 μm. Data are shown as mean ± s.d. **f**–**h**, The 14837T cells with *NUFIP1*-KO mCAFs, *NUFIP1*-WT mCAFs or *NUFIP1*-W35A mCAFs were orthotopically injected into mice, then the tumors were weighed ($n = 6$ mice) (**f**) and analyzed by Ki67 IHC staining ($n = 10$ views) (**g** and **h**). Scale bars, 20 μm. Data are shown as mean ± s.d. **i**, Orthotopic PDAC models in WT, *FSP-Cre;ATG5*$^{fl/fl}$ and *FSP-Cre;NUFIP1*$^{fl/fl}$ mice. After 14 d, TIF was obtained and metabolic analysis was performed. Data are shown as mean ± s.d. ($n = 6$ mice). **j**, The 14837T cells with different mCAFs orthotopically co-injected into mice. Then the tumors were analyzed by CK19 and *MYC* IHC staining. Scale bars, 30 μm. Representative images from three independent mice are shown. **k**, Orthotopic PDAC models in WT, *FSP-Cre;ATG5*$^{fl/fl}$ and *FSP-Cre;NUFIP1*$^{fl/fl}$ mice. The tumors were analyzed by CK19 and *MYC* IHC staining. Scale bars, 30 μm. Representative images from three independent mice are shown. **l**, The 14837T (WT) and 14837T (*MYC* knockdown) cells were orthotopically injected into WT and *FSP-Cre;NUFIP1*$^{fl/fl}$ mice. After 14 d, the tumors were weighed. Data are shown as mean ± s.d. ($n = 6$ mice). Statistical analysis was performed as in Fig. 7a. **m**, High expression (case 20) and low expression (case 27) of NUFIP1 in stroma. Scale bars, 20 μm. **n**, Survival curves for PDAC patients with low (blue) or high (red) stromal expression of NUFIP1. Statistical analysis was performed using the Gehan–Breslow–Wilcoxon test: $P = 4 \times 10^{-6}$, $n = 80$ patients. Statistical analysis was performed using ordinary one-way ANOVA with Tukey's multiple comparison test (**a**,**c**,**e**,**f**,**h**,**i**,**l**).

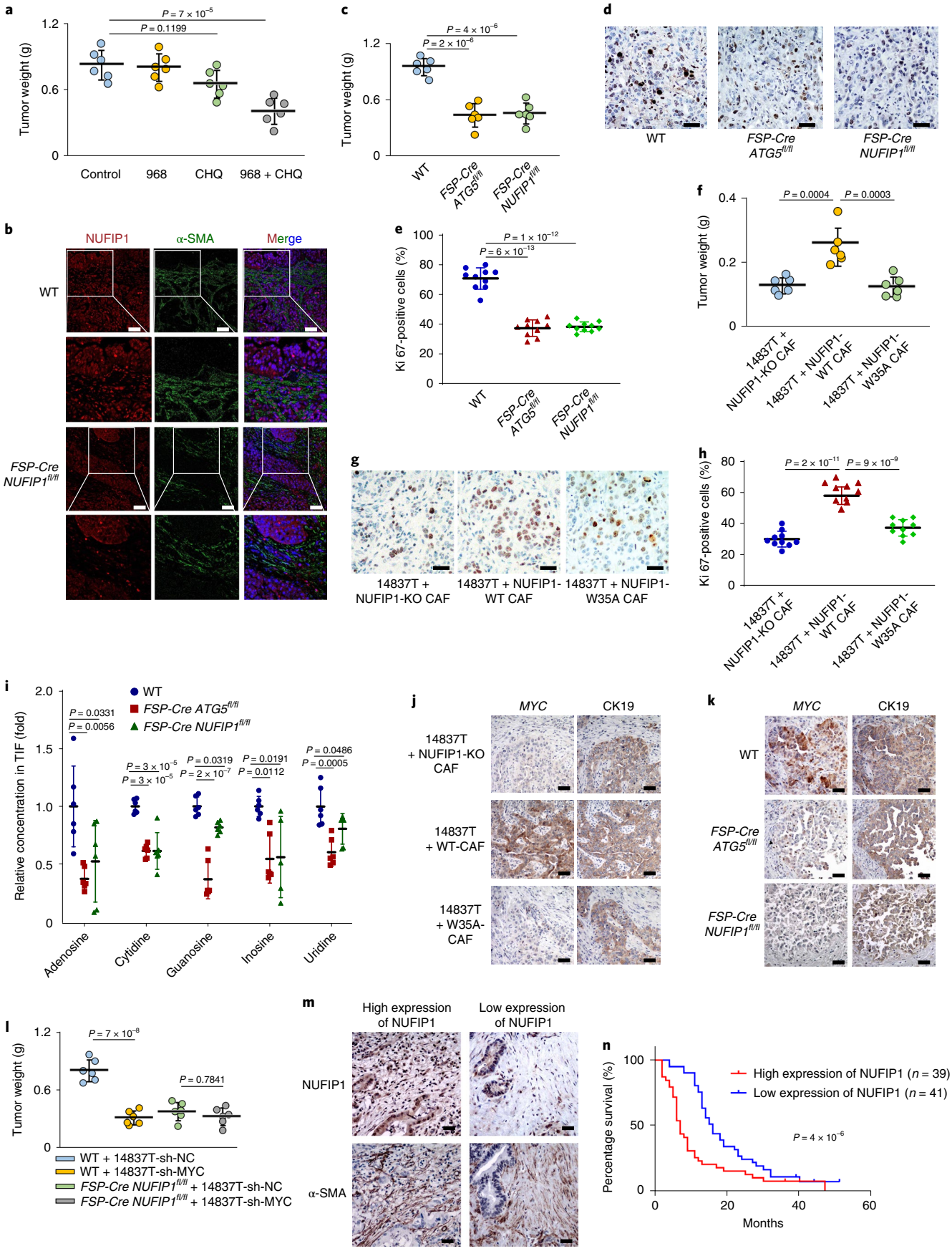
a
Tumor weight (g)
P = 7 × 10−5
P = 0.1199
Control
968
CHQ
968 + CHQ
b
NUFIP1
α-SMA
Merge
WT
FSP-Cre NUFIP1fl/fl
c
Tumor weight (g)
P = 4 × 10−6
P = 2 × 10−6
WT
FSP-Cre ATG5fl/fl
FSP-Cre NUFIP1fl/fl
d
WT
FSP-Cre ATG5fl/fl
FSP-Cre NUFIP1fl/fl
e
Ki 67-positive cells (%)
P = 1 × 10−12
P = 6 × 10−13
WT
FSP-Cre ATG5fl/fl
FSP-Cre NUFIP1fl/fl
f
Tumor weight (g)
P = 0.0004
P = 0.0003
14837T + NUFIP1-KO CAF
14837T + NUFIP1-WT CAF
14837T + NUFIP1-W35A CAF
g
14837T + NUFIP1-KO CAF
14837T + NUFIP1-WT CAF
14837T + NUFIP1-W35A CAF
h
Ki 67-positive cells (%)
P = 2 × 10−11
P = 9 × 10−9
14837T + NUFIP1-KO CAF
14837T + NUFIP1-WT CAF
14837T + NUFIP1-W35A CAF
i
Relative concentration in TIF (fold)
WT
FSP-Cre ATG5fl/fl
FSP-Cre NUFIP1fl/fl
P = 0.0331
P = 0.0056
P = 3 × 10−5
P = 3 × 10−5
P = 0.0319
P = 2 × 10−7
P = 0.0191
P = 0.0112
P = 0.0486
P = 0.0005
Adenosine
Cytidine
Guanosine
Inosine
Uridine
j
MYC
CK19
14837T + NUFIP1-KO CAF
14837T + WT-CAF
14837T + W35A-CAF
k
MYC
CK19
WT
FSP-Cre ATG5fl/fl
FSP-Cre NUFIP1fl/fl
l
Tumor weight (g)
P = 7 × 10−8
P = 0.7841
WT + 14837T-sh-NC
WT + 14837T-sh-MYC
FSP-Cre NUFIP1fl/fl + 14837T-sh-NC
FSP-Cre NUFIP1fl/fl + 14837T-sh-MYC
m
High expression of NUFIP1
Low expression of NUFIP1
NUFIP1
α-SMA
n
Percentage survival (%)
High expression of NUFIP1 (n = 39)
Low expression of NUFIP1 (n = 41)
P = 4 × 10−6
Months

secrete nucleosides to tumor cells in a *MYC*-dependent manner and delineate a role of CAF autophagy in controlling the tumor metabolic program.

Methods

Ethics approval and consent to participate. Mice (male/female) received standard chow diet freely and were housed in conditions of 12:12 h dark:light cycle, 22 ± 1 °C ambient temperature and 50 ± 10% humidity at Peking University Health Science Center animal facility. All animal experiments were performed in accordance with a protocol approved by the Department of Laboratory Animal Science of Peking University Health Science Center and supervised by the institutional review board of Peking University.

The primary tumor cell lines, hCAFs, human TMA samples were collected from PDAC patients (male/female) aged 34–82 years diagnosed with PDAC at the Department of Pancreatic Surgery, Huashan Hospital. All manipulations about human patient samples were approved by the Research Ethics Committee of Huashan Hospital, Fudan University. All patients provided written informed consent before enrollment and have consented to the data reporting provided in Supplementary Table 4.

Transgenic mice cell line. Primary mouse PDAC cell lines 14837T and 14838T were isolated as described[38] from genetically engineered C57BL/6 mice (tetO_LK ras^{G12D}p53$^{L/+}$p48-Cre)[39] and maintained in Dulbecco's modified Eagle's medium (DMEM) containing 10% fetal bovine serum (FBS) and 1 μg ml^{-1} of doxycycline.

Mouse models. Mice for fibroblast deletion of NUFIP1 or ATG5 were generated by breeding NUFIP1$^{fl/fl}$ mice and *ATG5*$^{fl/fl}$ mice with *FSP*-Cre mice (Shanghai Model Organisms Centre). *NUFIP1*$^{fl/fl}$ mice were ordered from Cyagen Biosciences. *ATG5*$^{fl/fl}$ mice were ordered from Shanghai Model Organisms Center. All genotyping was done by PCR.

Cell culture. The human pancreatic cancer cell lines 8988T, 8988S, MIA PaCa-2, PL45, HPAC, ASPC, PANC 03.27 and PANC-1 were grown in DMEM with 10% (v:v) FBS and the appropriate amount of penicillin–streptomycin in a 37 °C incubator with a humidified 5% CO_2 atmosphere.

The mCAFs were generated from C57BL/6J mice harboring mouse PDAC. These animals were pre-treated with a doxycycline diet and kept on a doxycycline regimen for the duration of the experiment, and were injected with 10^5 14837T or 14838T cells into the pancreas. Pancreatic tumors were resected at 2 weeks, mechanically minced and digested in collagenase and dispase. Cells were plated in cell culture dishes in DMEM with 10% FBS in the absence of doxycycline to limit the growth of *iKRAS* murine PDAC cells. The mCAFs were immortalized by infection with SV40 (Addgene, plasmid no. 22298) retroviruses.

The hCAFs were prepared by the outgrowth method. Fresh tissue was obtained from residual pancreatic adenocarcinoma specimens of patients undergoing primary surgical resection. It was digested in collagenase and dispase and mechanically minced. Primary human pancreatic CAFs were isolated by differential trypsinization and immortalized by infection with SV40 (Addgene, plasmid no. 298) retroviruses. Cells were kept in DMEM supplemented with 10% FBS.

CAFs were verified by measuring α*-SMA expression.* Primary hPDACs were obtained from PDAC patients surgery samples (hPDAC-1 is from a 58-year-old man with PDAC, hPDAC-2 is from a 62-year-old woman with PDAC). Tumor tissues were washed with phosphate-buffered saline (PBS) 2–3×. Then, 1 ml of digestive solution (1 mg ml^{-1} of type VIII collagenase (Sigma-Aldrich, catalog no. C2139), 2 mg ml^{-1} of dispase II (Sigma-Aldrich, catalog no. 4942078001), 1 mg ml^{-1} of trypsin inhibitor (Sigma-Aldrich, catalog no. T6522) and 1 unit ml^{-1} of DNase I (New England Biolabs, catalog no. M0303S) dissolved in PBS with 5% FBS) was added and digested at 37 °C for 40 min. The cell suspension was washed with PBS 1–2×. The supernatant was discarded by centrifugation and the cells were added to a 6-cm dish with fresh medium. Primary hPDACs were grown in DMEM with 10% (v:v) FBS and the appropriate amount of penicillin–streptomycin. We named the two primary human PDAC cells hPDAC-1 and hPDAC-2.

Plasmids. Complementary DNA of NUFIP1, c-myc and c-myc-3′-UTR were amplified and cloned into p3×Flag-CMV-10. After that, the cDNA of flag-NUFIP1, flag-c-myc and flag-c-myc-3′-UTR were cloned into lenti-EF1α-MCS-T2A-Hygro viral expression vector. The KO/knockdown (KD)-resistant plasmids are nonsense mutations of a clustered randomly regularly interspaced short palindromic repeats (CRISPR)–Cas9 sequence with a Fast mutagenesis kit (Vazyme). The NUFIP1-WT(r) and NUFIP1-W35A(r) plasmid sequence changes 'CCGCG GGACAACTGGGTGTACTGG' to 'CCGCGCGATAATTGGGTGTACGCG'. The flag-MYC(r) and flag-MYC-3′-UTR(r) plasmid sequence changes 'GACGAGAACAGTTGAAACA' to 'GATGAAAATAGCTGAAACA'.

Measurement of oxygen consumption. Oxygen consumption was monitored in 96-well-plate format using a phosphorescent oxygen-sensitive probe as previously described[40]. Briefly, cells were cultured and treated in 96-well plates. After appropriate treatment, 1 ml of reconstituted MitoXpress Xtra reagent was added to 15 ml of pre-warmed fresh culture medium; 150 μl of this solution was pipetted into each well of a 96-well plate. For drug treatments, compound stock solutions were prepared in dimethylsulfoxide (DMSO) and added to the wells to give the indicated final concentrations, maintaining the final DMSO concentration <0.5% (v:v). Finally, 100 μl of mineral oil was added to each well to seal the samples from ambient oxygen. Oxygen consumption was measured and processed according to instructions. OCRs were normalized for cell counts.

Immunofluorescence analysis. Cells were cultured in confocal plates. After appropriate treatment, cells were fixed with 4% paraformaldehyde and permeabilized with methanol. The confocal plates were incubated with blocking solution (0.8% bovine serum albumin in PBS) and exposed overnight to primary antibody (1:50 dilution for all antibodies) at 4 °C. After incubation for 2 h with secondary antibodies, samples were incubated with DAPI. Immunofluorescent images were obtained using a confocal microscope.

De-paraffined sections with 3-μm thickness were repaired by microwave. After that, the sections were treated with 0.5% Triton X-100 for 30 min and blocked with goat serum for 1 h at room temperature, washing with PBS 3× between each step. The sections were incubated with antibodies overnight at 4 °C in a humidified chamber, followed by incubation with secondary antibodies and DAPI, as mentioned earlier. Anti-fade mounting medium was used to seal the sections. Immunofluorescent images were obtained using a confocal microscope.

RNA immunoprecipitation. The NUFIP1-WT and NUFIP1-W35A plasmids of the viral expression vector were transfected into 293T cells. After 48 h, the virus-containing supernatant of these cultures was collected and concentrated. CAFs were infected with the viruses supplemented with 4 μg ml^{-1} of polybrene. The hygromycin selection (500 μg ml^{-1}) started 48 h after the infection and was continued for a week to generate stable cell pools. The cells were cultured in no glutamine medium for 48 h. Cells were then harvested after ultraviolet (UV) crosslinking (254-nm UV light 400 mJ cm^{-2}) and lysed on ice for 10 min with cold lysis buffer (50 mM Hepes, pH 7.5, 150 mM KCl, 2 mM EDTA, 0.5% NP-40, 0.5 mM dithiothreitol (DTT), 1× protease inhibitor, 100 U ml^{-1} of RNasin). Then the solution was centrifuged at 12,000*g* and 4 °C for 15 min, and the supernatant collected; 30 μl of M2 beads was added to the supernatant and the supernatant was incubated at 4 °C overnight with tumbling. The beads were washed with IP washing buffer (50 mM Hepes, pH 7.5, 300 mM KCl, 0.05% NP-40, 0.5 mM DTT) 5×. After that, the beads were resuspended in 100 μl of NT2 buffer (10 μl of DNase 2 U ml^{-1}, RNasin 100 U ml^{-1}) and incubated at 30 °C for 15 min; 1 ml of the NT2 buffer was added to the mixture, which was centrifuged at 1,000*g* and 4 °C for 5 min and the supernatant discarded. The beads were resuspended in 100 μl of NT2 buffer (1 μl of 10% sodium dodecylsulfate (SDS), 5 μl of proteinase K and RNasin 100 U ml^{-1}) and incubated at 55 °C for 15 min. NT2 buffer, 200 μl, was added, centrifuged at 1,000*g* and 4 °C for 5 min and the supernatant collected. To the supernatant was added 1 ml of TRIzol and the RNA was extracted. Sequences for qPCR primers are provided in Supplementary Table 1.

Purified autophagosome. The method of purifying autophagosome refers to the previous article[41]. Cells were collected and resuspended in pre-cold buffer (250 mM sucrose, 20 mM Hepes, pH 7.4, 1 mM EDTA and 1× protease inhibitor) and the cells were broken in a Dounce homogenizer using a pestle. The cells were centrifuged at 12,000*g* for 15 min to obtain the supernatant. A discontinuous OptiPrep gradient (Sigma-Aldrich, catalog no. D1556) was generated in an SW60 tube for ultracentrifuge rotors by overlaying the following OptiPrep solutions: 1 ml of 15% OptiPrep, 1 ml of 10% OptiPrep, 1 ml of 5% OptiPrep, 0.8 ml of 0% OptiPrep and the supernatant. The gradient was centrifuged at 150,200*g* in a Beckman SW60Ti rotor for 3 h with subsequent centrifugation of the fractions. The fractions were directly used for western blotting or RNA extraction.

Glucose uptake assay. Glucose uptake was measured with Glucose Uptake-Glo Assay kit (Promega, catalog no. J1341). Briefly, cells were cultured in 96-well plates. After the treatment, cells were washed twice with PBS; 1 mM 2-deoxy-D-glucose (2-DG) was added and the solution incubated for 10 min at room temperature. After this, the uptake of 2-DG was measured according to the kit instructions. Each analysis was standardized by cell number.

Sucrose gradient fractionation of ribosomes. About 1 × 10^7 cells were washed twice in cold PBS and lysed by 1.0 ml of polysome extraction buffer (20 mM Tris-HCl, pH 7.5, 100 mM KCl, 5 mM $MgCl_2$, 0.5% NP-40) containing 100 μg ml^{-1} of cycloheximide (CHX), 1× protease inhibitors and 1:1,000 dilution of RiboLock RNase inhibitor. The cell suspension was incubated on ice for 10 min and centrifuged at 12,000*g* for 15 min. The supernatant was collected and 300 μg of RNA was loaded on to 10–50% sucrose gradients. Tubes were centrifuged using a Beckman SW40Ti rotor at 190,000*g* for 1.5 h. Fractions were collected and mRNA was extracted with TRIzol. Analysis of mRNA distribution in the sucrose gradient was by qPCR.

Xenografts. Six-week-old C57BL/6J mice were used for tumorigenesis. These animals were pre-treated with a doxycycline diet and kept on a doxycycline

regimen for the duration of the experiment, and were injected with 10^5 14837T or 14838T cells into the pancreas. Briefly, an incision was made on the flank, above the spleen. The spleen was identified and gently pulled out through the incision to expose the pancreas. Then 20 µl of cell suspension was injected into the tail of the pancreas. The spleen and pancreas were carefully reintroduced into the animal and the peritoneum sutured. Then, 2 weeks after inoculation, the mice were killed, the tumors were weighed and the volume was measured. Maximal tumor burden (10% of body weight) and maximal tumor size (2.0 cm) allowed by the ethics committee were not exceeded. The drug was injected intraperitoneally, starting from day 5. The concentration of 968 is 5 mg kg^{-1} d^{-1} and that of CHQ is 60 mg kg^{-1} d^{-1}.

Tumor interstitial fluid. TIF was isolated according to the published methodology[42]. Tumor was taken from tumor-bearing mice and washed with saline (4 °C). The tumors were dried and centrifuged in a TIF isolation tube at 10,000,000*g* and 4 °C for 10 min. TIF was collected and quenched with 80% methanol. The samples were then used to measure metabolism.

Glucose and glutamine assay. Glucose detection kit (GOD-POD microplate method) (LEAGENE, catalog no. TC0711) was used to detect glucose level. Glutamine level was detected by ELISA kit (MEIMIAN, catalog no. MM-0863M2).

Metabolomics. Cells were washed with ice-cold saline, quenched with 80% methanol and subjected to three rapid freeze–thaw cycles. The debris was pelleted by centrifugation at 4 °C and the supernatant containing aqueous metabolites was collected and evaporated to dryness using a SpeedVac concentrator. Metabolites were reconstituted in 100 µl of 0.03% formic acid in analytical-grade water, vortexed and centrifuged to remove insoluble material. The supernatant was collected and subjected to targeted metabolomics analysis by ultra-performance liquid chromatography (LC) coupled with triple-quadrupole tandem mass spectrometry (MS).

Reagents. Uridine (catalog no. HZB1604-5) and inosine (catalog no. HZB1587-5) were purchased from HARVEYBIO, and adenosine (catalog no. A0152), guanosine (catalog no. G0171) and cytidine (catalog no. C0522) were purchased from TCI. Doxycycline (catalog no. S5159) was purchased from Selleck. CHQ (catalog no. C6628), 2-DG (catalog no. D8375) and MethADP (catalog no. M3763) were purchased from Sigma-Aldrich. Compound 968 (catalog no. HY-12682), actinomycin D (catalog no. HY-17559), dipyridamole (catalog no. HY-B0312), SCH58261 (catalog no. HY-19533), FCCP (catalog no. HY-100410) and rotenone (catalog no. HY-B1756) were purchased from MedChemExpress. Oligomycin (catalog no. O31530) was purchased from HARVEVBIO. Stable isotope-labeled nucleosides including [$^{13}C_5$]adenosine (catalog no. IR-25765) and [$^{13}C_5$]uridine (catalog no. IR-25790) were produced by Shanghai ZZBIO Co., Ltd. Stable isotope-labeled glucose, [$^{13}C_6$]glucose (catalog no. CLM-1396-1), was produced by Cambridge Isotope Laboratories.

Western blotting. Cells were harvested and then lysed in lysis buffer (1% NP-40, 150 mM NaCl, 50 mM Tris, pH 7.5, 5 mM EDTA, 0.05% SDS and 1% EDTA-free protease and phosphatase inhibitor cocktails; Roche Applied Science) on ice for 25 min. After centrifugation at 12,000 r.p.m. and 4 °C for 15 min, the protein concentration was measured with Coomassie brilliant blue (CBB). Equal amounts of proteins (20–40 µg) were size fractionated by 6–15% SDS–polyacrylamide gel electrophoresis. After transfer to nitrocellulose membranes or poly(vinylidene fluoride) membranes, the membranes were blocked with milk at room temperature for 1 h and incubated with primary antibody at 4 °C overnight, and the secondary antibody at room temperature for 1 h.

Gene expression analysis by RT–qPCR. Total RNA was extracted with TRIzol and reverse transcripted with 2 µg. Relative gene expression was determined by RT–PCR using an Applied Biosystems 7500 Real-Time PCR System according to the manufacturer's recommended protocol. Each analysis was performed in triplicate. Sequences for qPCR primers are provided in Supplementary Table 1.

Generation of CRISPR–Cas9 KO cell lines. The Cas9 KO cell lines were generated using CRISPR–Cas9 methods. We used the lentiCRISPRv2 puro vector purchased from Addgene (catalog no. 98290) and lentiCRISPRv.2 hygro vector purchased from Addgene (catalog no. 98291). The sgRNA was designed by online software (http://crispr.mit.edu). Lentiviruses were generated using pMDLg/pRRE (catalog no. 12251), pRSV-REV (catalog no. 12253) and pCMV-VSV-G (catalog no. 8454) vectors together with lentiCRISPRv.2. These plasmids were transfected into 293T cells and, after 48 h, the virus-containing supernatant of these cultures was collected and concentrated. Cells were infected with the lentiviruses supplemented with 4 µg ml^{-1} of polybrene. The puromycin selection (2.5 µg ml^{-1}) started 48 h after the infection and was continued for a week to generate stable cell pools. The sgRNA sequences are provided in Supplementary Table 2.

Lentiviral mRNA targets. Puromycin-resistance shRNA plasmids were purchased from Suzhou GenePharma. Tet-pLKO-neo was used to construct an inducible *slc2a1*-shRNA plasmid. *Slc2a1* knockdown was induced by treatment of doxycycline. The sequences for each shRNA are provided in Supplementary Table 3.

IHC staining. For IHC analysis, 3-mm sample sections were incubated with anti-Ki67 (1:1,000), anti-α-smooth muscle actin (SMA) (1:100), anti-NUFIP1 (1:50), anti-CK19 (1:1,000), anti-amylase (1:50) and anti-insulin (1:50) respectively, overnight at 4 °C in a humidified chamber, followed by incubation with the horseradish peroxidase-conjugated secondary antibodies at 37 °C for 30 min. Staining was completed by 1–2 min of incubation with diaminobenzidine substrate, which results in a brown-colored precipitate at the antigen site. The tissue sections stained immunohistochemically were analyzed and the mean staining intensity was calculated using Image-Pro Plus software.

Masson's Trichrome staining. Masson's Trichrome staining was used to detect fibrosis. De-paraffined sections with 5-µm thickness were stained according to instructions (Applygen, catalog no. B1130). Images were taken under uplight microscopy for analysis.

Statistics and reproducibility. Raw numerical data and statistical analysis of all repeats for all figures and Extended Data are provided in the Source data. Information about experimental replicates is included in the figure legends. Statistical analysis was performed using the SPSS statistical software package (standard v.20; SPSS Inc.). For two-group statistical analyses, unpaired Student's *t*-test was used. Error bars represent s.d., as indicated in the legends. For more than two-group statistical analyses, Dunnett's test were used.

Littermate animals from different cages were randomly assigned to the experimental groups. Tumor weight measurements were performed in a blinded manner. All other data collection and analysis were not performed blind to the conditions of the experiments. Data distribution was assumed to be normal but not formally tested. No data were excluded from the analyses.

No statistical method was used to predetermine sample size in all the highly controlled in vitro or in vivo experiments, but our sample sizes are similar to those reported in previous publications. For each experiment, we aimed for a number of at least of three samples or animals per group to allow basic statistical significance. The exact sample size was indicated in the figure legend. All animals were randomized and exposed to the same environment.

Reporting summary. Further information on research design is available in the Nature Research Reporting Summary linked to this article.

Data availability

The detailed results from the RNA-sequencing experiments are deposited in the National Center for Biotechnology Information's Gene Expression Omnibus (accession no. GSE185750). Metabolomics data have been deposited into MassIVE under accession no. MSV000089717. Source data are provided with this paper. All other data supporting the findings of the present study are available from the corresponding author on reasonable request.

Received: 6 October 2021; Accepted: 14 July 2022;
Published online: 18 August 2022

References

1. Pereira, B. A. et al. CAF subpopulations: a new reservoir of stromal targets in pancreatic cancer. *Trends Cancer* **5**, 724–741 (2019).
2. Hosein, A. N., Brekken, R. A. & Maitra, A. Pancreatic cancer stroma: an update on therapeutic targeting strategies. *Nat. Rev. Gastro. Hepatol.* **17**, 487–505 (2020).
3. Neuzillet, C. et al. Inter- and intra-tumoural heterogeneity in cancer-associated fibroblasts of human pancreatic ductal adenocarcinoma. *J. Pathol.* **248**, 51–65 (2019).
4. Klionsky, D. J. Autophagy: from phenomenology to molecular understanding in less than a decade. *Nat. Rev. Mol. Cell Biol.* **8**, 931–937 (2007).
5. Mizushima, N. Autophagy in protein and organelle turnover. *Cold Spring Harb. Symp. Quant. Biol.* **76**, 397–40 (2011).
6. Endo, S. et al. Autophagy Is required for activation of pancreatic stellate cells, associated with pancreatic cancer progression and promotes growth of pancreatic tumors in mice. *Gastroenterology* **152**, 1492–1506.e1424 (2017).
7. Sousa, C. M. et al. Pancreatic stellate cells support tumour metabolism through autophagic alanine secretion. *Nature* **536**, 479–483 (2016).
8. Zhang, X. B. et al. Blocking autophagy in cancer-associated fibroblasts supports chemotherapy of pancreatic cancer cells. *Front. Oncol.* **8**, 590 (2018).
9. Goruppi, S. et al. Autophagy controls CSL/RBPJ kappa stability through a p62/SQSTM1-dependent mechanism. *Cell Rep,* **24**, 3108–310 (2018).
10. Zhao, X. L. et al. High-mobility group box 1 released by autophagic cancer-associated fibroblasts maintains the stemness of luminal breast cancer cells. *J. Pathol.* **243**, 376–389 (2017).
11. Gatica, D., Lahiri, V. & Klionsky, D. J. Cargo recognition and degradation by selective autophagy. *Nat. Cell Biol.* **20**, 233–242 (2018).
12. Beese, C.J., Brynjolfsdottir, S.H. & Frankel, L.B. Selective autophagy of the protein homeostasis machinery: ribophagy, proteaphagy and ER-phagy. *Front. Cell Dev. Biol.* **7,** 373 (2020).

13. Wyant, G. A. et al. NUFIP1 is a ribosome receptor for starvation-induced ribophagy. *Science* **360**, 751–758 (2018).
14. Biancur, D. E. et al. Compensatory metabolic networks in pancreatic cancers upon perturbation of glutamine metabolism. *Nat. Commun.* **8**, 15965 (2017).
15. Son, J. et al. Glutamine supports pancreatic cancer growth through a KRAS-regulated metabolic pathway. *Nature* **496**, 101–105 (2013).
16. Lee, S. W. et al. EGFR-Pak signaling selectively regulates glutamine deprivation-induced macropinocytosis. *Dev. Cell* **50**, 381–392.e385 (2019).
17. An, H., Ordureau, A., Korner, M., Paulo, J. A. & Harper, J. W. Systematic quantitative analysis of ribosome inventory during nutrient stress. *Nature* **583**, 303–309 (2020).
18. Bardoni, B., Schenck, A. & Mandel, J. L. A novel RNA-binding nuclear protein that interacts with the fragile X mental retardation (FMR1) protein. *Hum Mol Genet* **8**, 2557–2566 (1999).
19. Itakura, E., Kishi-Itakura, C. & Mizushima, N. The hairpin-type tail-anchored SNARE syntaxin 17 targets to autophagosomes for fusion with endosomes/lysosomes. *Cell* **151**, 1256–1269 (2012).
20. Byun, J. K. et al. Oncogenic KRAS signaling activates mTORC1 through COUP-TFII-mediated lactate production. *EMBO Rep* **20**, e47451 (2019).
21. Kaadige, M. R., Looper, R. E., Kamalanaadhan, S. & Ayer, D. E. Glutamine-dependent anapleurosis dictates glucose uptake and cell growth by regulating MondoA transcriptional activity. *Proc. Natl Acad. Sci. USA* **106**, 14878–14883 (2009).
22. Hsieh, A. L., Walton, Z. E., Altman, B. J., Stine, Z. E. & Dang, C. V. MYC and metabolism on the path to cancer. *Semin. Cell Dev. Biol.* **43**, 11–21 (2015).
23. Dejure, F. R. et al. The MYC mRNA 3′-UTR couples RNA polymerase II function to glutamine and ribonucleotide levels. *EMBO J.* **36**, 1854–1868 (2017).
24. Rudnick, J. A. et al. Autophagy in stromal fibroblasts promotes tumor desmoplasia and mammary tumorigenesis. *Genes Dev.* **35**, 963–975 (2021).
25. Lyssiotis, C. A. & Kimmelman, A. C. Metabolic interactions in the tumor mcroenvironment. *Trends Cell Biol.* **27**, 873–885 (2017).
26. Yang, L. F. et al. Targeting stromal glutamine synthetase in tumors disrupts tumor microenvironment-regulated cancer cell growth. *Cell Metab.* **24**, 685–700 (2016).
27. Mishra, R. et al. Stromal epigenetic alterations drive metabolic and neuroendocrine prostate cancer reprogramming. *J. Clin. Invest.* **128**, 4472–4484 (2018).
28. Zhu, Z. W. et al. Tumour-reprogrammed stromal BCAT1 fuels branched-chain ketoacid dependency in stromal-rich PDAC tumours. *Nat. Metab.* **2**, 775–77 (2020).
29. Blobel, G. & Potter, V. R. Studies on free and membrane-bound ribosomes in rat liver. I. Distribution as related to total cellular RNA. *J. Mol. Biol.* **26**, 279–27 (1967).
30. Tajan, M. et al. A role for p53 in the adaptation to glutamine starvation through the expression of SLC1A3. *Cell Metab.* **28**, 721–72 (2018).
31. Tardito, S. et al. Glutamine synthetase activity fuels nucleotide biosynthesis and supports growth of glutamine-restricted glioblastoma. *Nat. Cell Biol.* **17**, 1556–1568 (2015).
32. Linker, W., Loffler, M. & Schneider, F. Uridine, but not cytidine can sustain growth of Ehrlich ascites tumor cells in glucose-deprived medium with altered proliferation kinetics. *Eur. J. Cell Biol.* **36**, 176–181 (1985).
33. Hessmann, E., Schneider, G., Ellenrieder, V. & Siveke, J. T. MYC in pancreatic cancer: novel mechanistic insights and their translation into therapeutic strategies. *Oncogene* **35**, 1609–1618 (2016).
34. Goetzman, E. S. & Prochownik, E. V. The role for Myc in coordinating glycolysis, oxidative phosphorylation, glutaminolysis, and fatty acid metabolism in normal and neoplastic tissues. *Front. Endocrinol.* **9**, 129 (2018).
35. Wise, D. R. et al. Myc regulates a transcriptional program that stimulates mitochondrial glutaminolysis and leads to glutamine addiction. *Proc. Natl Acad. Sci. USA* **105**, 18782–18787 (2008).
36. Lao-On, U. et al. c-Myc directly targets an over-expression of pyruvate carboxylase in highly invasive breast cancer. *Biochem. Biophys. Acta Mol. Basis Dis.* **1866**, 165656 (2020).
37. Yuneva, M., Zamboni, N., Oefner, P., Sachidanandam, R. & Lazebnik, Y. Deficiency in glutamine but not glucose induces MYC-dependent apoptosis in human cells. *J. Cell Biol.* **178**, 93–105 (2007).
38. Aguirre, A. J. et al. Activated Kras and Ink4a/Arf deficiency cooperate to produce metastatic pancreatic ductal adenocarcinoma. *Genes Dev.* **17**, 3112–3126 (2003).
39. Ying, H. et al. Oncogenic Kras maintains pancreatic tumors through regulation of anabolic glucose metabolism. *Cell* **149**, 656–670 (2012).
40. Hynes, J. et al. Investigation of drug-induced mitochondrial toxicity using fluorescence-based oxygen-sensitive probes. *Toxicol. Sci.* **92**, 186–200 (2006).
41. Uematsu, M., Nishimura, T., Sakamaki, Y., Yamamoto, H. & Mizushima, N. Accumulation of undegraded autophagosomes by expression of dominant-negative STX17 (syntaxin 17) mutants. *Autophagy* **13**, 1452–1464 (2017).
42. Sullivan, M. R., Lewis, C. A. & Muir, A. Isolation and quantification of metabolite levels in murine tumor interstitial fluid by LC/MS. *Bio. Protoc.* **9**, e3427 (2019).

Acknowledgements

The present study was supported by the National Key R&D Program of China (nos. 2017YFA0503900 and 2019YFC1005200 to Y.Z.), National Natural Science Foundation of China (nos. 82173020, 81874145 and 81672712 to Y.Z.) and Peking University (nos. BMU2022XKQ004 and PKU2020LCXQ024 to Y.Z.).

Author contributions

M.Y. carried out in vitro cell experiments, in vivo experiments, manuscript preparation, IHC analysis and statistical analysis. T.B., N.Z., M.F., J.B., W.W., Z.S. S.H., J.Z. and L.W. carried out in vitro cell experiments and in vivo experiments. H.P., K.Y. and Z.H. carried out metabolism experiments and analyzed the data. H.L. and D.F. provided clinical specimens. C.D. contributed to manuscript preparation. W.G.Z supervised the study. Y.Z. conceived, designed and supervised the study and wrote the manuscript.

Competing interests

The authors declare no competing interests.

Additional information

Extended data Extended data are available for this paper at https://doi.org/10.1038/s43018-022-00426-6.

Supplementary information The online version contains supplementary material available at https://doi.org/10.1038/s43018-022-00426-6.

Correspondence and requests for materials should be addressed to Deliang Fu, Zeping Hu or Ying Zhao.

Peer review information *Nature Cancer* thanks the anonymous reviewers for their contribution to the peer review of this work.

Reprints and permissions information is available at www.nature.com/reprints.

Publisher's note Springer Nature remains neutral with regard to jurisdictional claims in published maps and institutional affiliations.

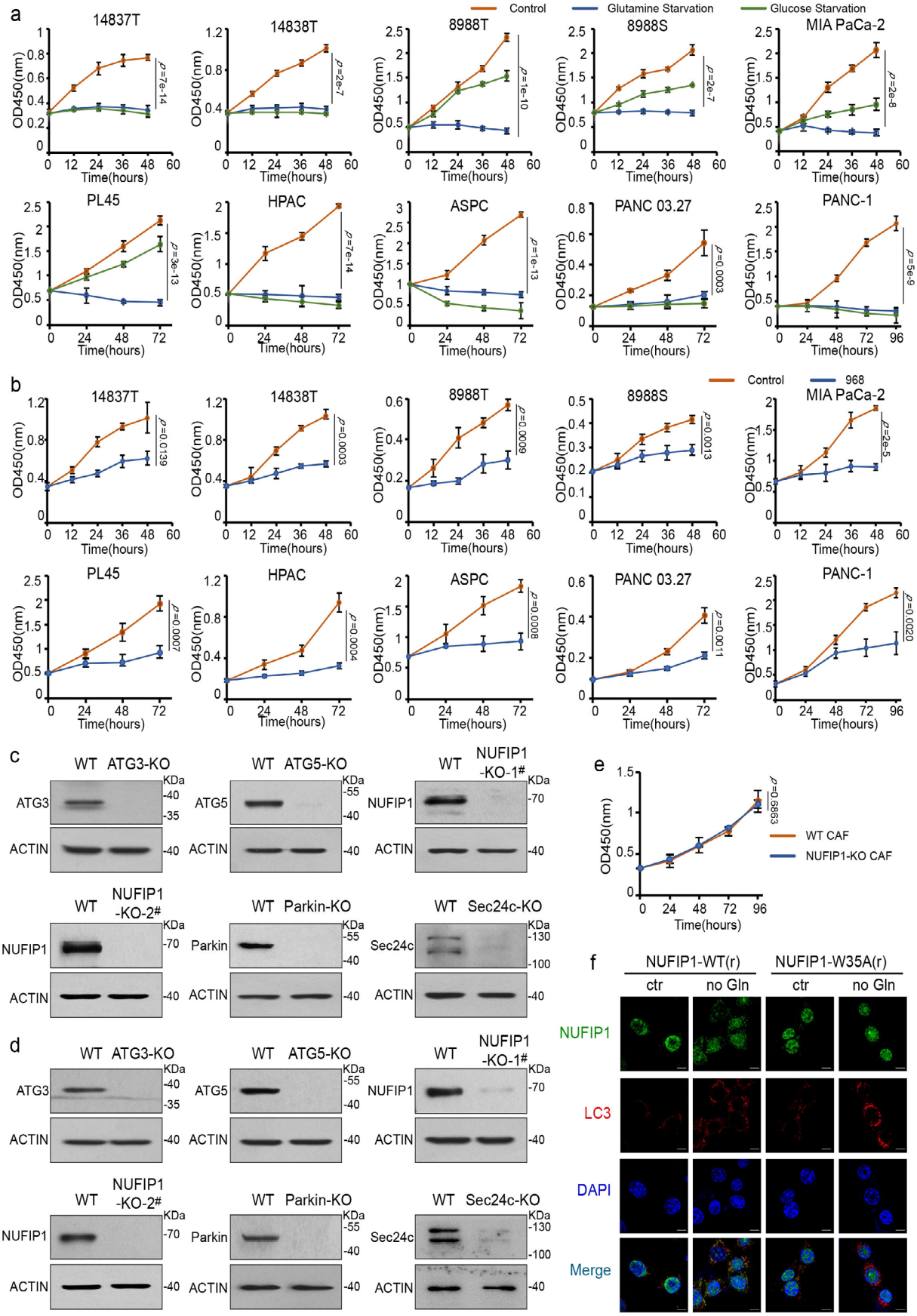

Extended Data Fig. 1 | See next page for caption.

Extended Data Fig. 1 | PDAC cells were sensitive to glutamine starvation. (a) Cell growth rate was detected by MTT assay. 14837 T, 14838 T, 8988 T, 8988 S, MIA Paca-2, PL45, HPAC, ASPC, PANC 03.27 and PANC-1 cells were incubated in complete media (25 mM glucose, 4 mM glutamine), no glucose media or no glutamine media. The absorbance at 450 nm was measured at different time points. Data are shown as mean ± SD (n = 3 independent samples). Statistical analysis was performed using ordinary one-way ANOVA with Tukey's multiple comparisons test. **(b)** Cell growth rate was detected by MTT assay. 14837 T, 14838 T, 8988 T, 8988 S, MIA Paca-2, PL45, HPAC, ASPC, PANC 03.27 and PANC-1 cells were incubated with or without 968 (20 μM). The absorbance at 450 nm was measured at different time points. Data are shown as mean ± SD (n = 3 independent samples). **(c, d)** Knock-out cell lines of mCAFs or hCAFs were obtained by CRISPR/Cas9 technique. Western blotting was used to detect the knockout efficiency of mCAFs(c) and hCAFs(d). Experiments in c, d were repeated every 2 weeks, with similar results. **(e)** Cell growth rate was detected by MTT assay. mCAFs and NUFIP1-KO mCAFs cells were incubated with no glutamine media. The absorbance at 450 nm was measured at different time points. Data are shown as mean ± SD (n = 3 biologically independent samples). **(f)** CRISPR/Cas9-resistent NUFIP1-WT(r) and NUFIP1-W35A(r) were overexpressed in NUFIP1-KO mCAFs. These cells were cultured with or without glutamine for 48 h, and then immunostained with the antibody against NUFIP1 and LC3. The results showed the cellular localization of NUFIP1. Scale bars: 5 μM. Representative of n = 3 independent experiments. Pairwise comparisons were conducted using two-tailed, unpaired Student's t-tests (b, e).

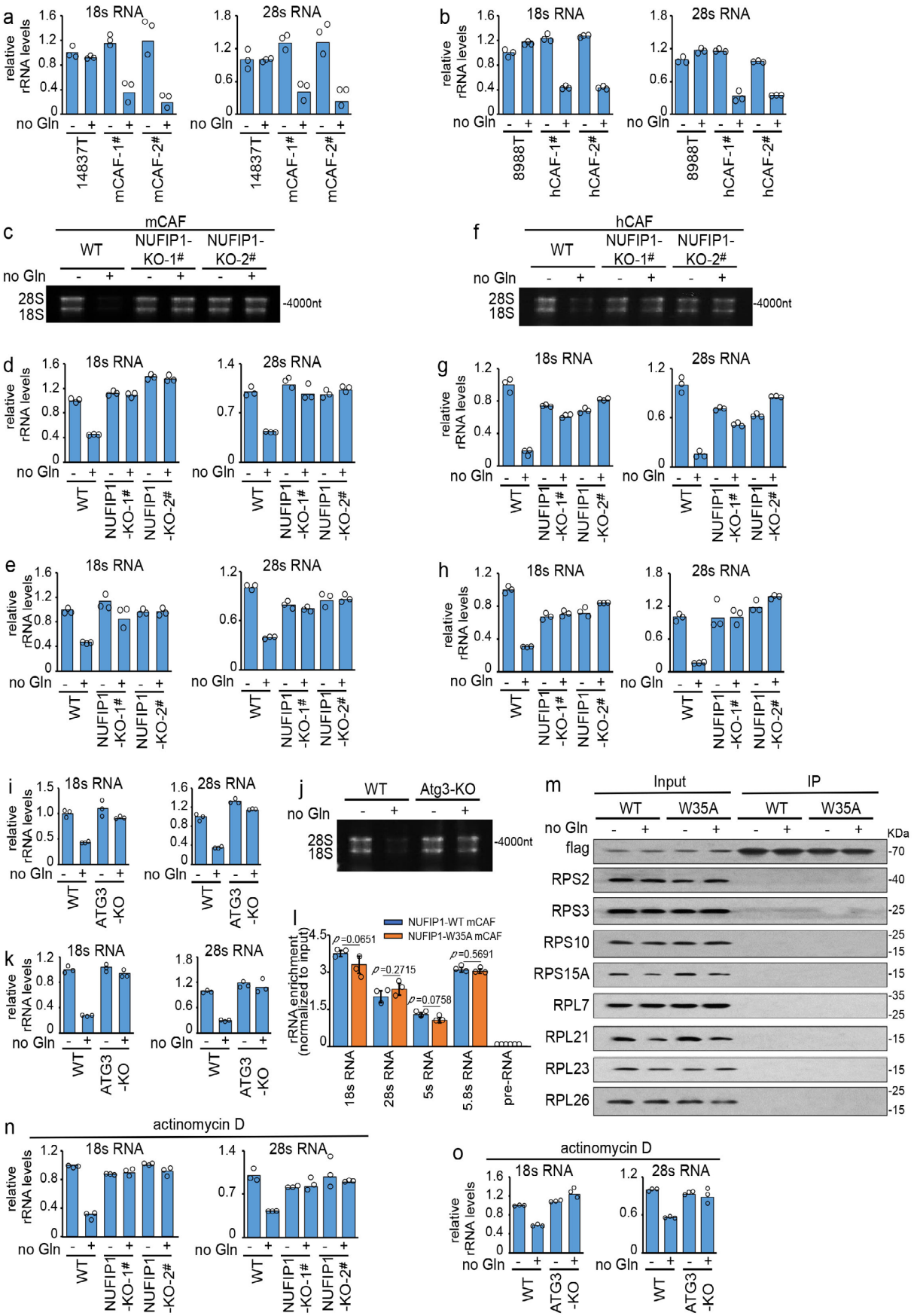

Extended Data Fig. 2 | See next page for caption.

Extended Data Fig. 2 | rRNA degradation is activated in CAFs. (a, b) Cells were cultured with or without glutamine for 48 h. RNA was analyzed with RT-PCR and normalized to GAPDH. **(c)** mCAF-2# was cultured with or without glutamine for 48 h. RNA gel showed the degradation of RNA. Representative of n = 3 independent experiments. **(d, e)** mCAF-1#(d) and mCAF-2# (e) were cultured with or without glutamine for 48 h. RNA was analyzed with RT-PCR and normalized to GAPDH. **(f)** hCAF-2# was cultured with or without glutamine for 48 h. RNA gel showed the degradation of RNA. Representative of n = 3 independent experiments. (g-i) hCAF-1#**(g)**, hCAF-2# **(h)** or autophagy-deficient mCAFs **(i)** were cultured with or without glutamine for 48 h. RNA was analyzed with RT-PCR and normalized to GAPDH. **(j, k)** Wild-type or autophagy-deficient hCAFs were cultured with or without glutamine for 48 h. RNA gel showed the degradation of RNA **(j)**. Representative of n = 3 independent experiments. RNA was also analyzed with RT-PCR and normalized to GAPDH **(k)**. **(l)** 14837 T infected with virus of flag-NUFIP1-WT or flag-NUFIP1-W35A was immunoprecipitated using M2 beads. The co-precipitated RNAs were purified and analyzed by RT-qPCR using primers for the indicated RNA species. The relative rRNA level was normalized to the input. Data are shown as mean ± SD (n = 3 independent experiments). Pairwise comparisons were conducted using two-tailed, unpaired Student's t-tests. **(m)** 14837 T infected with virus of Flag-NUFIP1-WT and Flag-NUFIP1-W35A for 48 h and cultured with or without glutamine for 48 h. Then cells were immunoprecipitated using M2 beads. The co-precipitation proteins were detected by WB. Representative of n = 3 independent experiments. (n-o) WT mCAFs, *NUFIP1*-KO mCAFs(n) or autophagy-deficient mCAFs (o) were cultured with or without glutamine for 48 h under actinomycin D treatment. RNA was analyzed with RT-PCR and normalized to GAPDH. Data are shown as mean ± SD (3 times the experiment was repeated with similar results) (a, b, d, e, g-i, k, n, o).

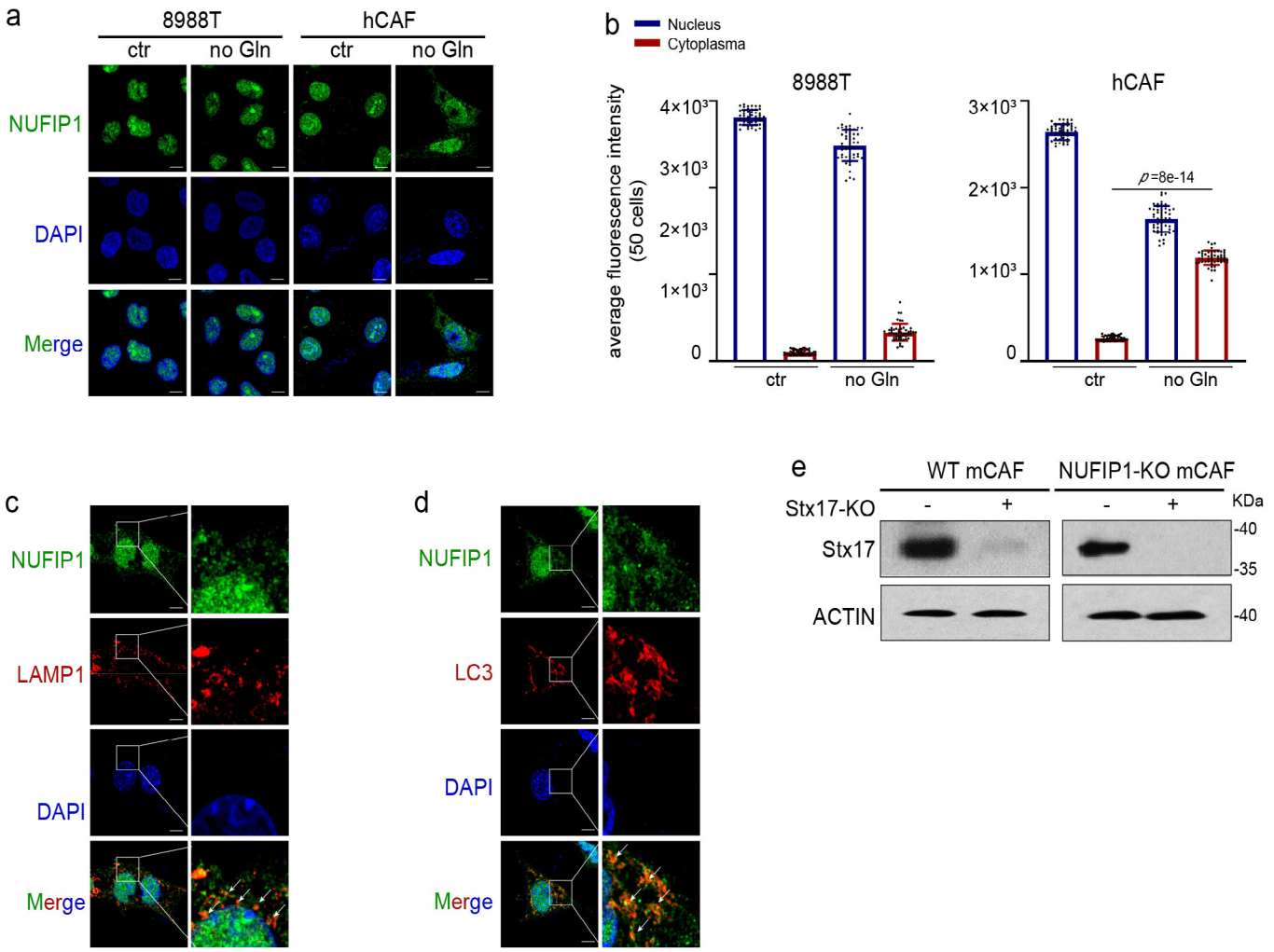

Extended Data Fig. 3 | NUFIP1 translocated from the nucleus to the cytoplasm. (a, b) 8988 T and hCAFs were cultured with or without glutamine for 48 h and then immunostained with the antibody against NUFIP1. The results showed the cellular localization of NUFIP1 in 8988 T and hCAFs. Scale bars: 5 μM. Representative of n = 3 independent experiments. The average fluorescence intensity of NUFIP1 in nucleus and cytoplasm were recorded **(b)**. Data are shown as mean ± SD (n = 50 cells). Statistical analysis was performed using ordinary one-way ANOVA with Tukey's multiple comparisons test. **(c, d)** hCAFs were treated with no glutamine media for 48 h. These cells were immunostained with the antibody against NUFIP1, LAMP1 or LC3. The results showed the co localization of NUFIP1 with LAMP1 (c) or LC3 (d). The white arrows point to the co localization of the described protein. Scale bars: 5 μM. Representative of n = 3 independent experiments. **(e)** STX17-KO mCAFs and NUFIP1/STX17 double-KO mCAFs were obtained by CRISPR/Cas9 technique. Western blotting was used to detect the knockout efficiency. Representative of n = 3 independent experiments.

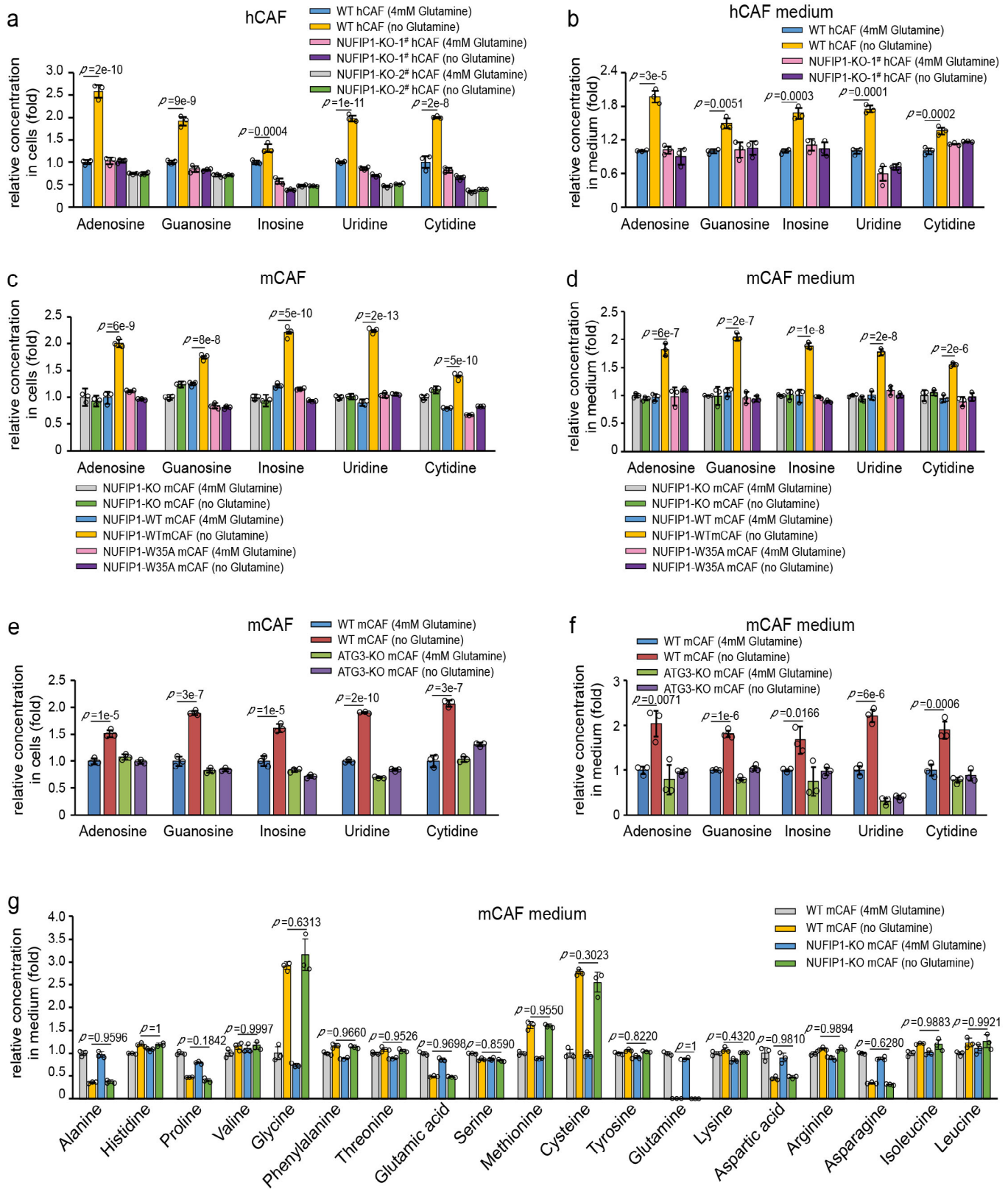

Extended Data Fig. 4 | See next page for caption.

Extended Data Fig. 4 | CAFs secrete nucleosides dependent on NUFIP1. (a, b) Relative content of nucleosides in cells (a) and medium (b). WT hCAFs and NUFIP1-KO hCAFs were cultured with or without glutamine for 48 h. Metabolic analysis of cells was performed by mass spectrometry. Data are shown as mean ± SD (n = 3 biologically independent samples). **(c, d)** Relative content of nucleosides in cells (c) and medium (d). NUFIP1-KO mCAFs, NUFIP1-WT mCAFs and NUFIP1-W35A mCAFs were cultured with or without glutamine for 48 h. Metabolic analysis of cells was performed by mass spectrometry. Data are shown as mean ± SD (n = 3 biologically independent samples). **(e, f)** Relative content of nucleosides in cells (e) and medium (f). WT mCAFs and *Atg3*-KO mCAFs were cultured with or without glutamine for 48 h. Metabolic analysis of cells was performed by mass spectrometry. Data are shown as mean ± SD (n = 3 biologically independent samples). (g) Relative content of AA in cells. WT mCAFs and *NUFIP1*-KO mCAFs were cultured with or without glutamine for 48 h. Metabolic analysis of cells was performed by mass spectrometry. Data are shown as mean ± SD (n = 3 biologically independent samples). Statistical analysis was performed using ordinary one-way ANOVA with Tukey's multiple comparisons test (a-g).

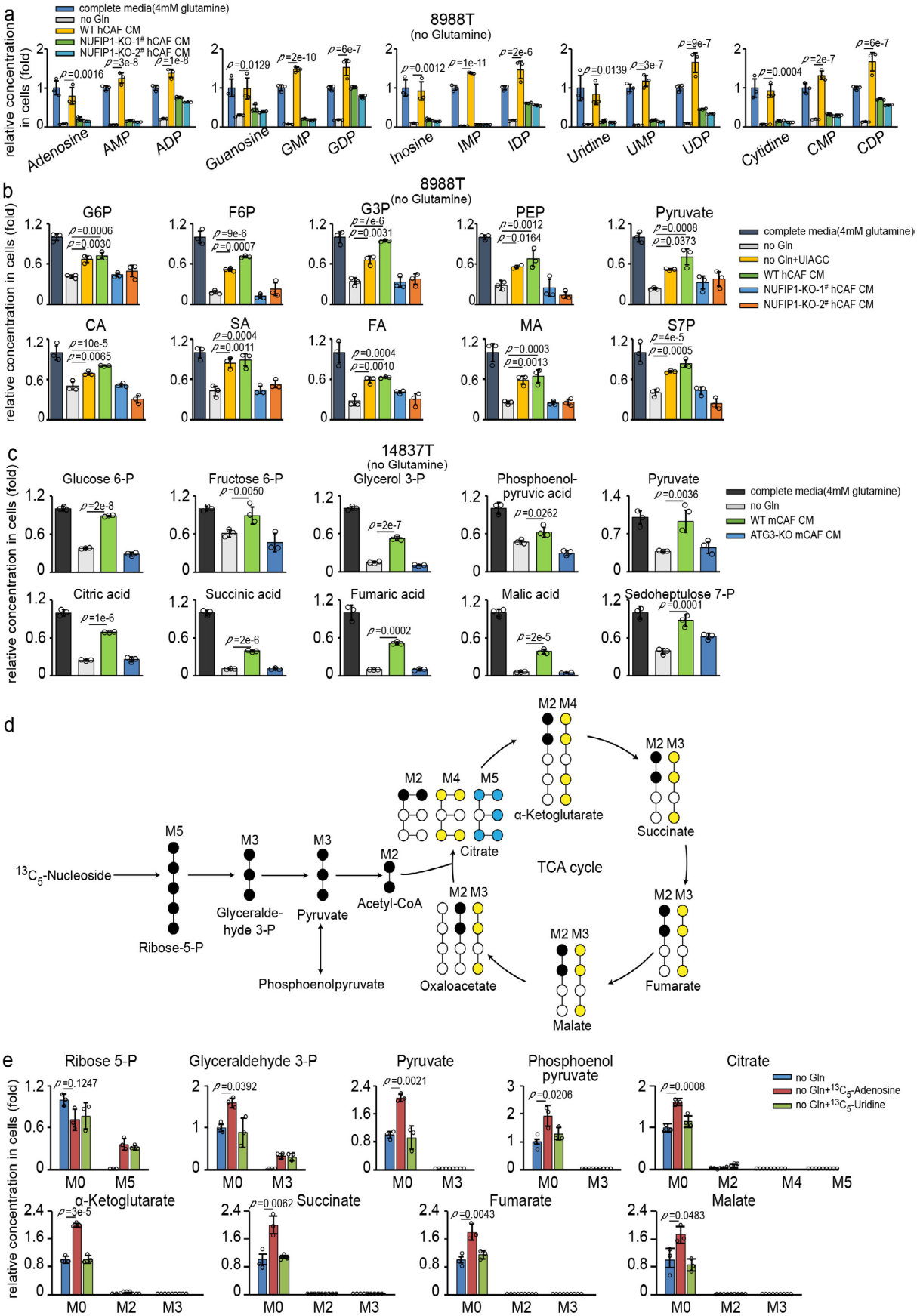

Extended Data Fig. 5 | See next page for caption.

Extended Data Fig. 5 | CAFs secrete nucleosides that promote PDAC metabolism. (a) 8988 T cells were cultured in complete media (4 mM glutamine) or conditioned medium (no glutamine) from different cell lines for 48 h. Nucleosides and nucleotides in the cells were analyzed by mass spectrometry. Data are shown as mean ± SD (one representative of three independent experiments with similar results is shown). **(b)** 8988 T cells were cultured in complete media (4 mM glutamine), no glutamine media with or without UIAGC (0.5 mM each) or conditioned medium (no glutamine) from WT hCAFs and *NUFIP1*-KO hCAFs for 48 h. Metabolic analysis of cells was performed by mass spectrometry. Data are shown as mean ± SD (one representative of three independent experiments with similar results is shown). **(c)** 14837 T cells were cultured in complete media (4 mM glutamine), no glutamine media or conditioned medium (no glutamine) from WT mCAFs and *Atg3*-KO mCAFs for 48 h. Metabolic analysis of cells was performed by mass spectrometry. Data are shown as mean ± SD (one representative of three independent experiments with similar results is shown). **(d)** Metabolic map of stable isotope tracer experiment in Extended Data Fig. 5e. **(e)** 14837 T cells were cultured in no glutamine media with or without $^{13}C_5$-Adenosine (2 mM) or $^{13}C_5$-Uridine (2 mM) for 48 h. ^{13}C stable isotope labeled the ribose in nucleoside. The metabolites labeled with stable isotope in cells were detected by mass spectrometry. Data are shown as mean ± SD (one representative of three independent experiments with similar results is shown). Statistical analysis was performed using ordinary one-way ANOVA with Tukey's multiple comparisons test. (a-c, e).

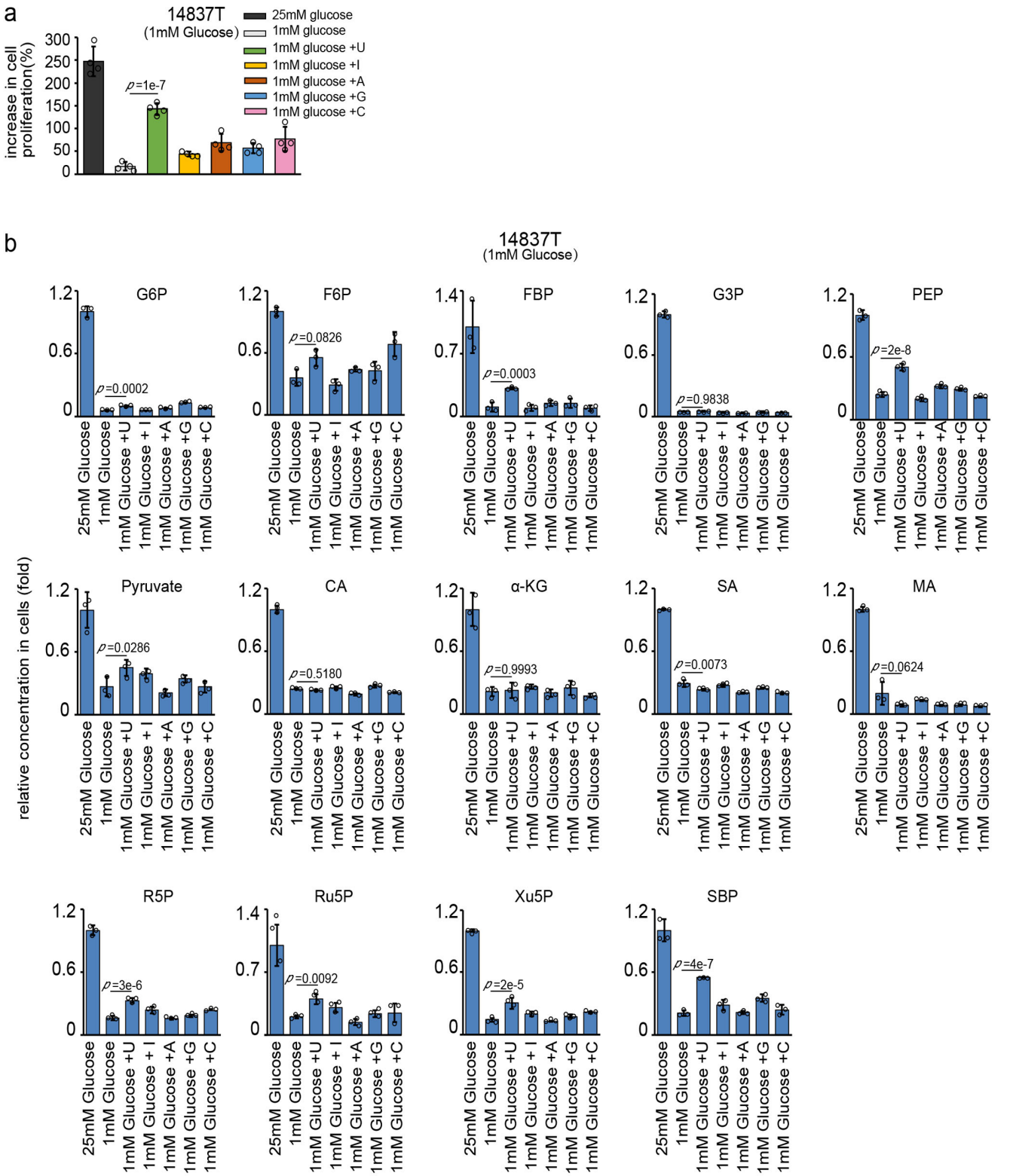

Extended Data Fig. 6 | Glycolysis and the TCA cycle were slightly affected by nucleosides under low glucose conditions. (a, b) 14837 T cells were cultured in complete media (25 mM glucose), low glucose media (1 mM glucose) with or without uridine (U, 0.5 mM), inosine (I, 0.5 mM), adenosine (A, 0.5 mM), guanosine (G, 0.5 mM), cytidine (C, 0.5 mM) for 48 h. The cells were counted to calculate the cell proliferation (a). Metabolic analysis of cells was performed by mass spectrometry (b). Data are shown as mean ± SD. (n = 3 biologically independent samples). Statistical analysis was performed using ordinary one-way ANOVA with Tukey's multiple comparisons test.

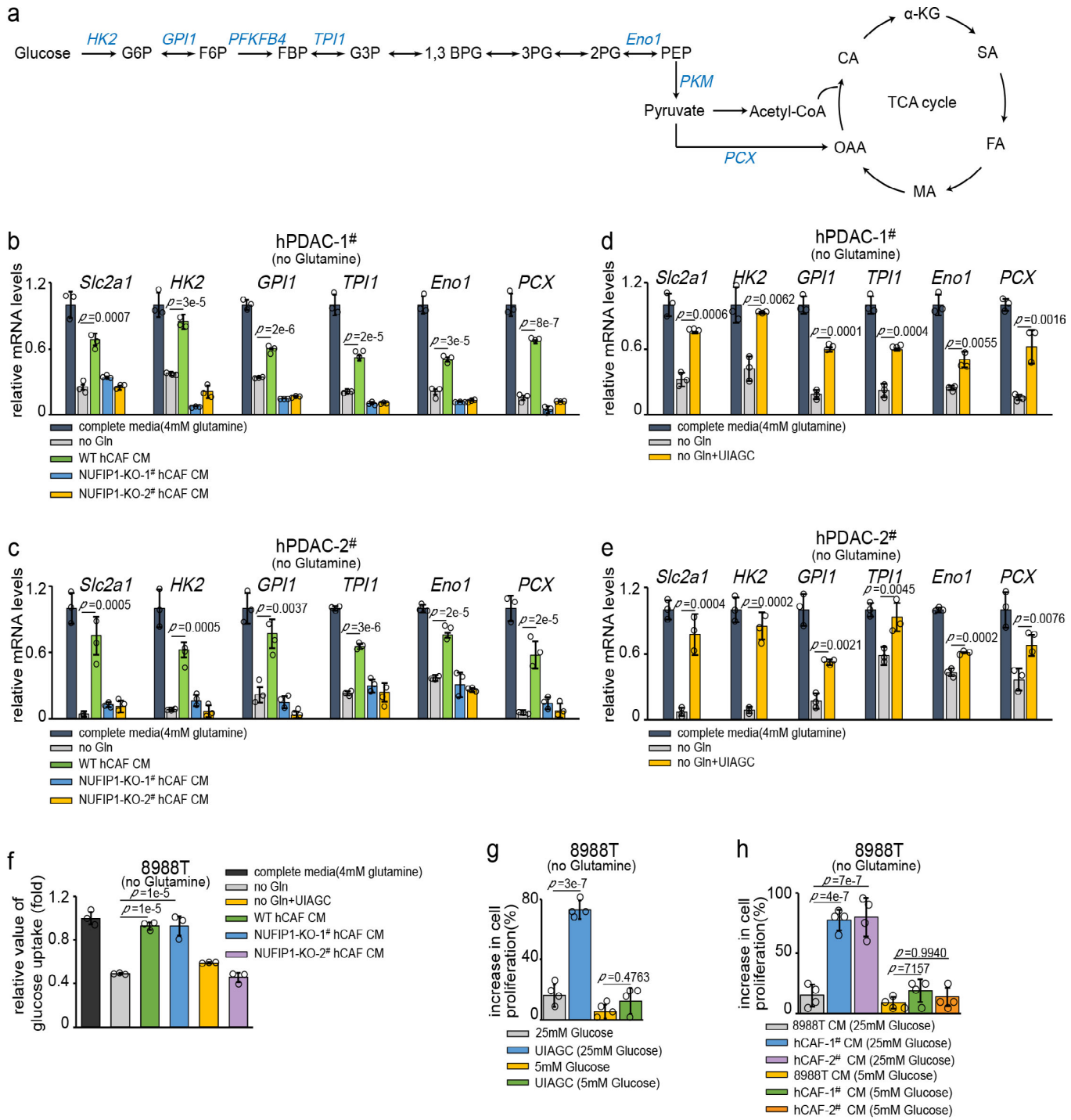

Extended Data Fig. 7 | The CAF-CM and nucleosides induced glucose consumption genes expression in PDAC. (a) Diagram of metabolic enzymes in the glycolysis pathway and TCA cycle. **(b, c)** hPDAC-1# and hPDAC-2# were cultured in complete media (4 mM glutamine) or conditioned medium (no glutamine) from different cell lines for 48 h. RNA was then extracted and analyzed with RT-PCR. Data are shown as mean ± SD (n = 3 independent experiments). **(d, e)** hPDAC-1# and hPDAC-2# were cultured in complete media (4 mM glutamine), no glutamine media with or without UIAGC (0.5 mM each) for 48 h. RNA was then extracted and analyzed with RT-PCR. Data are shown as mean ± SD (n = 3 independent experiments). **(f)** 8988 T cells were cultured in 96 well plates with complete media (4 mM glutamine), no glutamine media with UIAGC (0.5 mM each) or conditioned medium (no glutamine) from different cell lines for 48 h. The relative value of glucose uptake was measured by the Glucose Uptake-Glo™ Assay kit. Data are shown as mean ± SD (n = 3 biologically independent samples). **(g)** 8988 T cells were cultured in different media (no glutamine, 25 mM glucose or 5 mM glucose) with or without UIAGC (0.5 mM each) for 48 h. The cells were counted to calculate the cell proliferation. Data are shown as mean ± SD (n = 4 independent samples). **(h)** 8988 T cells were cultured in conditioned medium (no glutamine, 25 mM glucose or 5 mM glucose) from different cell lines with for 48 h. The cells were counted to calculate the cell proliferation. Data are shown as mean ± SD (n = 4 independent samples). Statistical analysis was performed using ordinary one-way ANOVA with Tukey's multiple comparisons test (b-h).

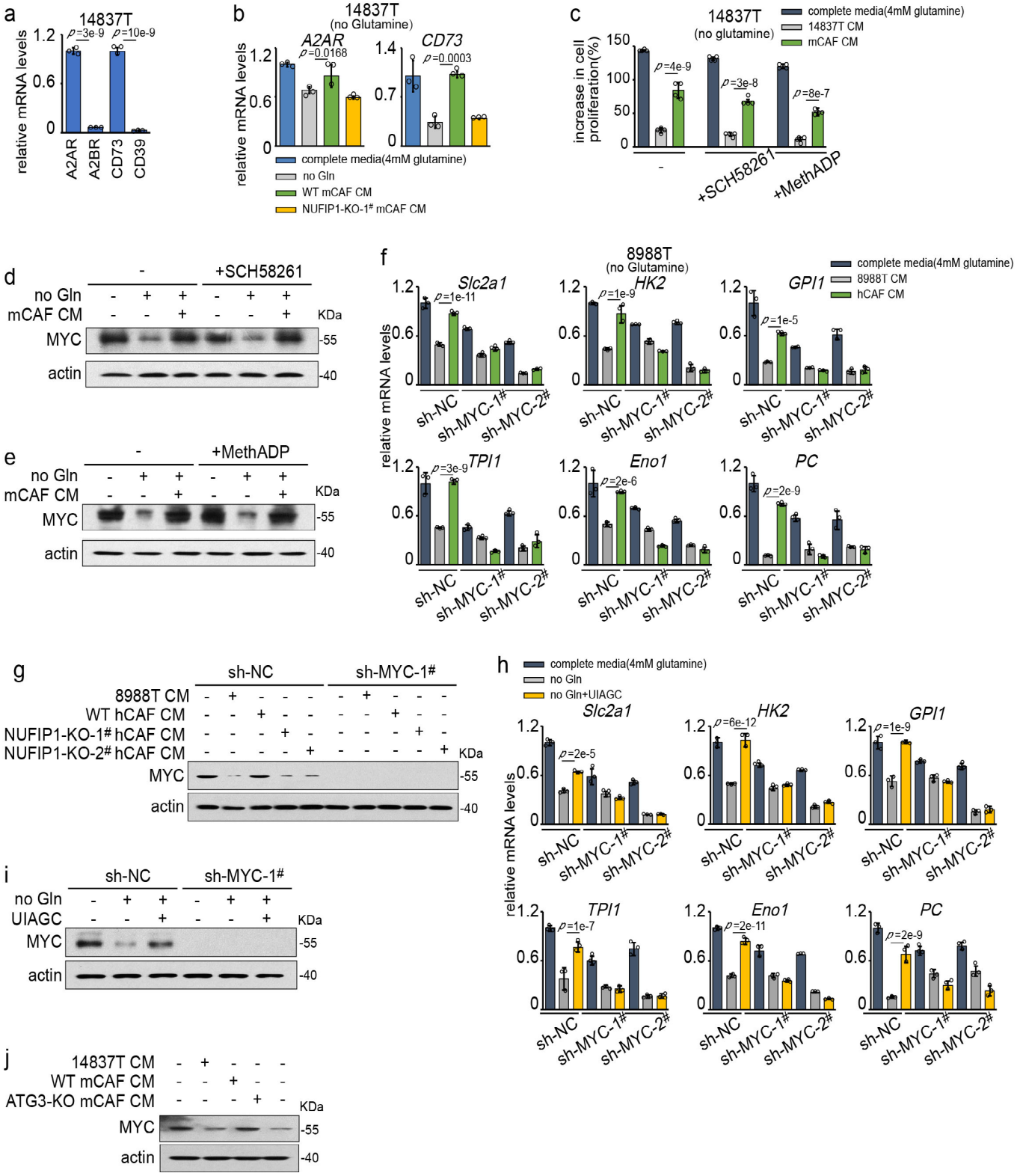

Extended Data Fig. 8 | See next page for caption.

Extended Data Fig. 8 | CAFs activate glucose consumption genes expression in PDAC dependent on MYC. (a) mRNA levels of A2AR, A2BR, CD73 and CD39 in 14837 T cells. Data are shown as mean ± SD (n = 3 independent experiments). **(b)** 14837 T cells were cultured in complete media (4 mM glutamine) or conditioned medium (no glutamine) from different cell lines for 48 h. RNA was extracted and analyzed with RT-PCR. Data are shown as mean ± SD (n = 3 independent experiments). (c-e) Detect the effects of A2AR inhibitor (SCH58261, 1 μM) and CD73 inhibitor (MethADP, 50 μM) on 14837 T. 14837 T cells were treated with SCH58261 (1 μM) or MethADP (50 μM) and cultured in complete media or conditioned medium (no glutamine) from 14837 T or mCAFs for 48 h. The cells were counted **(c)**. Data are shown as mean ± SD (n = 4 independent samples). WB was performed to determine MYC **(d, e)**. Representative of n = 3 independent experiments. (f-g) 8988 T and 8988 T (MYC knocked-down) cells were cultured in complete media or conditioned medium (no glutamine) from different cell lines for 48 h. RNA was then extracted and analyzed with RT-PCR **(f)**. Data are shown as mean ± SD (n = 3 independent experiments). WB was performed to determine MYC **(g)**. Representative of n = 3 independent experiments. (h-i) 8988 T (WT) and 8988 T (MYC knocked-down) cells were cultured in complete media or no glutamine media with or without UIAGC (0.5 mM each) for 48 h. RNA was then extracted and analyzed with RT-PCR **(h)**. Data are shown as mean ± SD (n = 3 independent experiments). WB was performed to determine MYC **(i)**. Representative of n = 3 independent experiments. **(j)** 14837 T cells were cultured in complete media (4 mM glutamine), no glutamine media or conditioned medium (no glutamine) from WT mCAFs and *Atg3*-KO mCAFs for 48 h. Western blotting was performed to determine MYC protein levels. Representative of n = 3 independent experiments. Statistical analysis was performed using ordinary one-way ANOVA with Tukey's multiple comparisons test. (a-c, f, h).

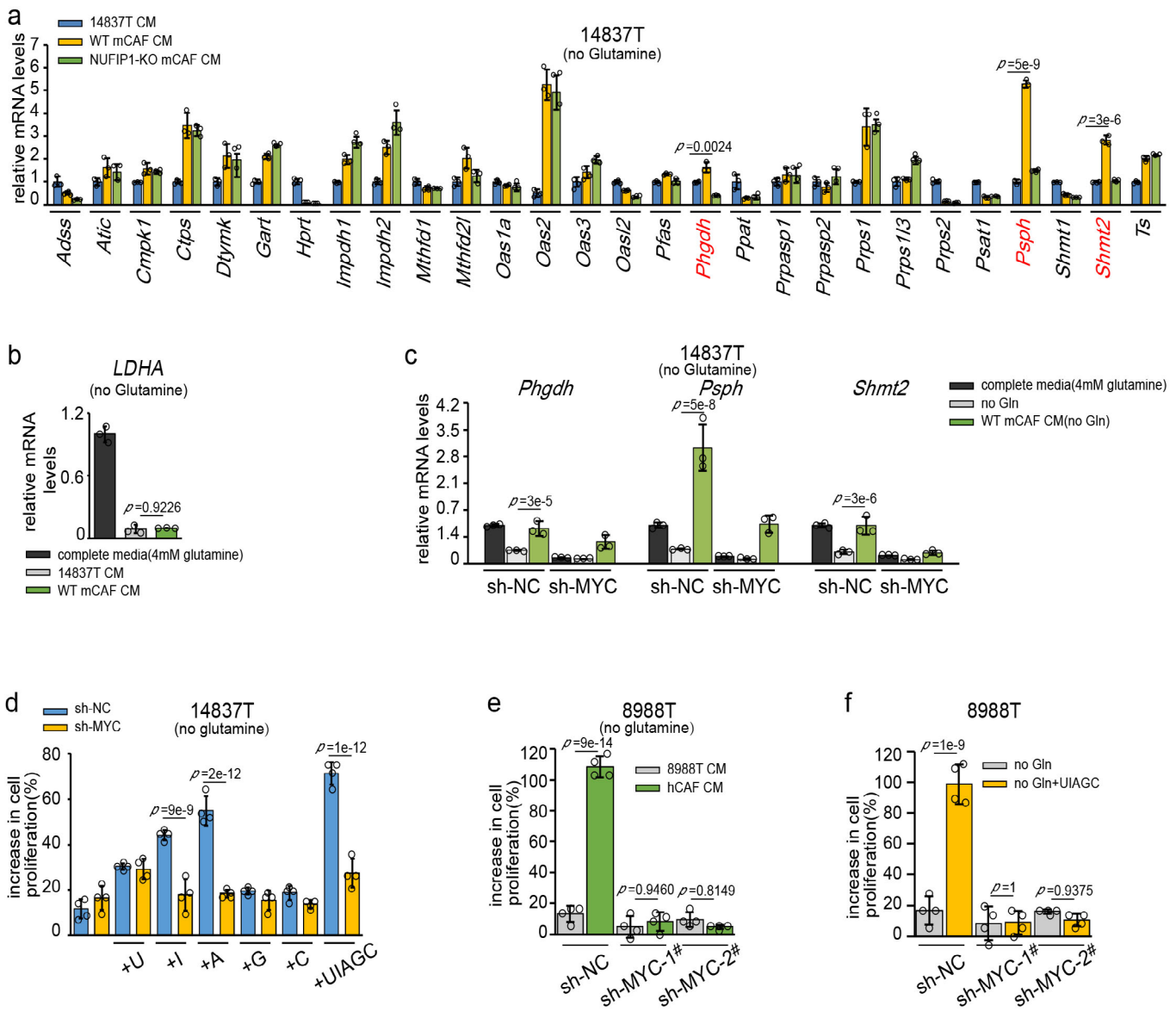

Extended Data Fig. 9 | CAFs promote growth of PDAC dependent on MYC. (a) 14837 T cells were cultured in conditioned medium (no glutamine) from different cell lines for 48 h. RNA was then extracted and analyzed with RT-PCR. Data are shown as mean ± SD (n = 3 independent experiments). **(b)** 14837 T cells were cultured in complete media (4 mM glutamine) or conditioned medium (no glutamine) from different cell lines for 48 h. RNA was then extracted and analyzed with RT-PCR. Data are shown as mean ± SD (n = 3 independent experiments). **(c)** 14837 T (WT) and 14837 T (MYC knocked-down) cells were cultured in complete media (4 mM glutamine) or conditioned medium (no glutamine) from 14837 T or mCAFs for 48 h. RNA was then extracted and analyzed with RT-PCR. Data are shown as mean ± SD (n = 3 independent experiments). **(d)** 8988 T and 8988 T (MYC knocked-down) cells were cultured in no glutamine media with or without uridine (U, 0.5 mM), inosine (I, 0.5 mM), adenosine (A, 0.5 mM), guanosine (G, 0.5 mM), cytidine (C, 0.5 mM) and UIAGC (0.5 mM each) for 48 h. Then cells were counted. Data are shown as mean ± SD (n = 4 independent samples). **(e)** 8988 T and 8988 T (MYC knocked-down) cells were cultured in conditioned medium (no glutamine) from 8988 T or hCAFs for 48 h. Then cells were counted. Data are shown as mean ± SD (n = 4 independent samples). **(f)** 8988 T and 8988 T (MYC knocked-down) cells were cultured in no glutamine media with or without UIAGC for 48 h. Then cells were counted. Data are shown as mean ± SD (n = 4 independent samples). Statistical analysis was performed using ordinary one-way ANOVA with Tukey's multiple comparisons test(a-f).

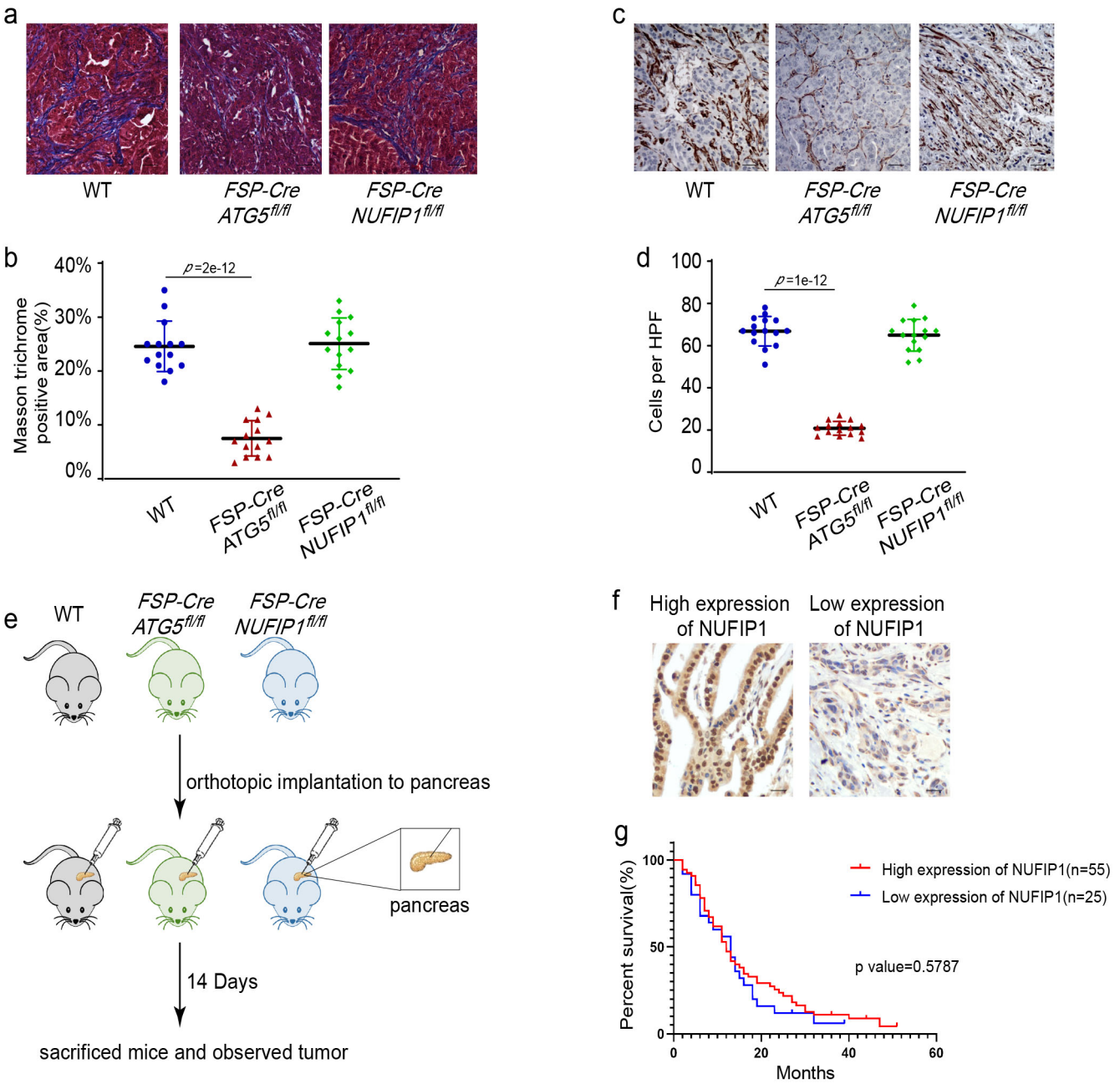

Extended Data Fig. 10 | NUFIP1 does not affect the desmoplastic response in PDAC. (a-d) 14837 T cells were orthotopically injected into WT, *FSP-Cre;ATG5*$^{fl/fl}$ and *FSP-Cre;NUFIP1*$^{fl/fl}$ mice. After 14 days, the tumors were analyzed by Masson trichrome staining (n = 14 views per group) **(a, b)** and α-SMA immunohistochemical staining (n = 15 views per group) **(c, d)**. Representative images are shown. Scale bars: 20 μM. Data are shown as mean ± SD. Statistical analysis was performed using ordinary one-way ANOVA with Tukey's multiple comparisons test. **(e)** Diagram of orthotopic syngeneic graft model in *FSP-Cre;ATG5*$^{fl/fl}$ and *FSP-Cre;NUFIP1*$^{fl/fl}$ mice. **(f)** High expression of NUFIP1 (case34) and low expression of NUFIP1 (case7) in tumor was shown. Scale bars: 10 μM. **(g)** Kaplan-Meier survival curves for PDAC patients with low (blue) or high (red) tumor expression of NUFIP1, as assessed by IHC. Statistical analysis was performed using Gehan–Breslow–Wilcoxon test; n = 80 patients.

nature portfolio

Corresponding author(s): Ying Zhao

Last updated by author(s): Jun 12, 2022

Reporting Summary

Nature Portfolio wishes to improve the reproducibility of the work that we publish. This form provides structure for consistency and transparency in reporting. For further information on Nature Portfolio policies, see our Editorial Policies and the Editorial Policy Checklist.

Statistics

For all statistical analyses, confirm that the following items are present in the figure legend, table legend, main text, or Methods section.

n/a	Confirmed
☐	☒ The exact sample size (*n*) for each experimental group/condition, given as a discrete number and unit of measurement
☐	☒ A statement on whether measurements were taken from distinct samples or whether the same sample was measured repeatedly
☐	☒ The statistical test(s) used AND whether they are one- or two-sided *Only common tests should be described solely by name; describe more complex techniques in the Methods section.*
☐	☒ A description of all covariates tested
☐	☒ A description of any assumptions or corrections, such as tests of normality and adjustment for multiple comparisons
☐	☒ A full description of the statistical parameters including central tendency (e.g. means) or other basic estimates (e.g. regression coefficient) AND variation (e.g. standard deviation) or associated estimates of uncertainty (e.g. confidence intervals)
☐	☒ For null hypothesis testing, the test statistic (e.g. *F*, *t*, *r*) with confidence intervals, effect sizes, degrees of freedom and *P* value noted *Give P values as exact values whenever suitable.*
☐	☒ For Bayesian analysis, information on the choice of priors and Markov chain Monte Carlo settings
☐	☒ For hierarchical and complex designs, identification of the appropriate level for tests and full reporting of outcomes
☒	☐ Estimates of effect sizes (e.g. Cohen's *d*, Pearson's *r*), indicating how they were calculated

Our web collection on statistics for biologists contains articles on many of the points above.

Software and code

Policy information about availability of computer code

Data collection	Image collection was performed with confocal microscope (ZEISS LSM880 laser scanning confocal microscope and ZEISS ZEN software). Quantitative RT-PCR (qRT-PCR) results were recorded with Applied Biosystems 7500 according to the manufacturer's instructions.
Data analysis	The tissue sections stained immunohistochemically were analyzed and the mean staining intensity was calculated using Image-Pro Plus software. The oligonucleotide primers for qRT-PCR were designed using LightCycler Probe Design Software 2.0 (Roche) or Primer Bank (http://pga.mgh.harvard.edu/primerbank/index.html). Statistical analysis was performed by using the SPSS statistical software package (standard version 20; SPSS Inc., Chicago, IL, USA).

For manuscripts utilizing custom algorithms or software that are central to the research but not yet described in published literature, software must be made available to editors and reviewers. We strongly encourage code deposition in a community repository (e.g. GitHub). See the Nature Portfolio guidelines for submitting code & software for further information.

Data

Policy information about availability of data

All manuscripts must include a data availability statement. This statement should provide the following information, where applicable:

- Accession codes, unique identifiers, or web links for publicly available datasets
- A description of any restrictions on data availability
- For clinical datasets or third party data, please ensure that the statement adheres to our policy

The detailed results from the RNA-Seq experiments are deposited in the NCBI's Gene Expression Omnibus (GEO GSE185750).

Metabolomics data have been deposited into MassIVE under accession code MSV000089717.

Field-specific reporting

Please select the one below that is the best fit for your research. If you are not sure, read the appropriate sections before making your selection.

☒ Life sciences ☐ Behavioural & social sciences ☐ Ecological, evolutionary & environmental sciences

For a reference copy of the document with all sections, see nature.com/documents/nr-reporting-summary-flat.pdf

Life sciences study design

All studies must disclose on these points even when the disclosure is negative.

Sample size	No statistical method was used to predetermine sample size in all the highly controlled in vitro or in vivo experiments, but our sample sizes are similar to those reported in previous publications. For each experiment, we aimed for a number of at least three samples or animals per group to allow basic statistical significance. The exact sample size was indicated in the figure legend.
Data exclusions	no data was excluded from the analyses
Replication	the experimental findings were successfully replicated a minimum of three times with similar results
Randomization	The in vitro experiments were not randomized. For the in vivo experiments, littermate animals from different cages were randomly assigned to the experimental groups.
Blinding	Tumor weihgt measurements were performed in a blinded manner. All other data collection and analysis were not performed blind to the conditions of the experiments,, but data were analyzed by multiple investigators, including those not involved in the experiment.

Reporting for specific materials, systems and methods

We require information from authors about some types of materials, experimental systems and methods used in many studies. Here, indicate whether each material, system or method listed is relevant to your study. If you are not sure if a list item applies to your research, read the appropriate section before selecting a response.

Materials & experimental systems

n/a	Involved in the study
☐	☒ Antibodies
☐	☒ Eukaryotic cell lines
☒	☐ Palaeontology and archaeology
☐	☒ Animals and other organisms
☐	☒ Human research participants
☒	☐ Clinical data
☒	☐ Dual use research of concern

Methods

n/a	Involved in the study
☒	☐ ChIP-seq
☒	☐ Flow cytometry
☒	☐ MRI-based neuroimaging

Antibodies

Antibodies used	The antibodies used were anti-ATG3 (MBL, #M133-3, 1:1000), anti-ATG5 (Novus, #NB110-53818, 1μg/ml), anti-actin (ZSGB-BIO, #TA-09, 1:10000), anti-LC3 for WB (CST, #2775S, 1:1000), anti-NUFIP1 (proteintech, #12515-1-AP, 0.8μg/ml), anti-Parkin (CST, #2132S, 1:1000), anti-Sec24c (proteintech, #16073-1-AP, 0.133μg/ml), anti-RPL7 (Bethyl, #A300-741A-M, 1:1000), anti-RPS15A (Bethyl, #A304-990A-M, 1:1000), anti-RPL21 (Bethyl, #A305-032A-M, 1:1000), anti-RPL23 (Bethyl, #A305-008A-M, 1:1000), RPL26 (Bethyl, #A300-686A-M, 1:1000), anti-RPS2 (ABclonal, #WH162144, 1:1000), anti-RPS3 (proteintech, #11990-1-AP, 0.4μg/ml), anti-LAMP1 for WB (proteintech, #21997-1-AP, 0.65μg/ml), anti-LAMP1 for IF (Sino Biological, #11215-MM07, 1:200), anti-LC3 for IF (MBL, #M152-3, 1:200), anti-p-p70S6K (CST, #9205S, 1:1000), anti-p70S6K (Bethyl, #A300-510A, 1:1000), anti-KRAS (Biodragon, #BD-PT5739, 1:1000), anti-c-myc (Santa Cruz, #9E10, 1μg/ml), anti-slc2a1 (proteintech, #21829-1-AP, 0.6μg/ml), anti-Ki67 (Abcam, #ab16667, 0.03μg/ml), anti-α-SMA (Gene Tech, #GM085129, 1:100), anti-CK19 (proteintech, #10712-1-AP, 0.5μg/ml)anti-c-myc (ZSGB-BIO, #ZA-0555, 1:1) and anti-flag(sigma, #F1804, 1μg/ml).
Validation	All antibodies have been validated for use in their respective applications (western blot, immunofluorescence and immunohistochemistry), as staged on the manufacturers' product pages. Anti-ATG3 (MBL, #M133-3): suitable for WB. Reacts with human and mouse. mCAFs and hCAFs whole cell lysate were used as a positive control. ATG3-KO cell lysate was used as a negative control. Anti-ATG5 (Novus, #NB110-53818): suitable for WB. Reacts with human and mouse. mCAFs and hCAFs whole cell lysate were used as a positive control. ATG5-KO cell lysate was used as a negative control. Anti-actin (ZSGB-BIO, #TA-09): suitable for WB. Reacts with human and mouse. 14837T, 14838T, mCAFs, 8988T, MIA Paca-2 and hCAFs whole cell lysate were used as a positive control.

Anti-LC3 (CST, #2775S): suitable for WB. Reacts with mouse. 14837T whole cell lysate was used as a positive control.
Anti-LC3 (MBL, #M152-3): suitable for IF. Reacts with human and mouse.
Anti-NUFIP1 (proteintech, #12515-1-AP): suitable for WB, IF and IHC. Reacts with human and mouse. mCAFs and hCAFs whole cell lysate were used as a positive control. NUFIP1-KO cell lysate was used as a negative control. FSP-Cre;NUFIP1fl/fl mice was used as a negative control for IHC.
Anti-Parkin (CST, #2132S): suitable for WB. Reacts with human and mouse. mCAFs and hCAFs whole cell lysate were used as a positive control. Parkin-KO cell lysate was used as a negative control.
Anti-Sec24c (proteintech, #16073-1-AP): suitable for WB. Reacts with human and mouse. mCAFs and hCAFs whole cell lysate were used as a positive control. Parkin-KO cell lysate was used as a negative control.
Anti-RPS15A (Bethyl, #A304-990A-M): suitable for WB. Reacts with mouse. Ribosome extract purified from mCAFs was used as a positive control.
Anti-RPL21 (Bethyl, #A305-032A-M): suitable for WB. Reacts with mouse. Ribosome extract purified from mCAFs was used as a positive control.
Anti-RPL23 (Bethyl, #A305-008A-M): suitable for WB. Reacts with mouse. Ribosome extract purified from mCAFs was used as a positive control.
Anti-RPL26 (Bethyl, #A300-686A-M): suitable for WB. Reacts with mouse. Ribosome extract purified from mCAFs was used as a positive control.
Anti- RPS2 (ABclonal, #WH162144): suitable for WB. Reacts with mouse. Ribosome extract purified from mCAFs was used as a positive control.
Anti-RPS3 (proteintech, #11990-1-AP): suitable for WB. Reacts with mouse. Ribosome extract purified from mCAFs was used as a positive control.
Anti-RPS10 (proteintech, #14894-1-AP): suitable for WB. Reacts with mouse. Ribosome extract purified from mCAFs was used as a positive control.
Anti-LAMP1 (proteintech, #21997-1-AP): suitable for WB. Reacts with mouse. Lysosomal extract purified from mCAFs was used as a positive control.
Anti-LAMP1 (Sino Biological, #11215-MM07): suitable for IF. Reacts with human and mouse.
Anti-p-p70S6K (CST, #9205S): suitable for WB. Reacts with human and mouse. Regulation of p-p70S6K expression by nutrient concentration was used as a positive and negative control.
Anti-p70S6K (Bethyl, #A300-510A): suitable for WB. Reacts with human and mouse. 14837T, 14838T, mCAFs, 8988T, MIA Paca-2 and hCAFs whole cell lysate were used as a positive control.
Anti-KRAS (Biodragon, #BD-PT5739): suitable for WB. Reacts with mouse. Regulation of KRAS expression with or without doxy was used as a positive or negative control.
Anti-c-myc (Santa Cruz, #9E10): suitable for WB. Reacts with human and mouse. 14837T and 8988T whole cell lysate were used as a positive control. sh-MYC cell lysate was used as a negative control.
Anti-c-myc (ZSGB-BIO, #ZA-0555): suitable for IHC. Reacts with mouse.
Anti-slc2a1 (proteintech, #21829-1-AP): suitable for WB. Reacts with human. 8988T whole cell lysate were used as a positive control. sh-slc2a1 cell lysate was used as a negative control.
Anti-Ki67 (Abcam, #ab16667): suitable for IHC. Reacts with mouse.
Anti-α-SMA (Gene Tech, #GM085129): suitable for IF and IHC. Reacts with human and mouse.
Anti-CK19 (proteintech, #10712-1-AP): suitable for IHC. Reacts with mouse.

Eukaryotic cell lines

Policy information about cell lines

Cell line source(s)	Primary mouse PDAC lines 14837T and 14838T were isolated from genetically engineered C57BL/6 mice (tetO_LKrasG12D, p53 L/+, p48-Cre). 8988T, 8988S, MIA PaCa-2, PL45, HPAC, BxPC-3, ASPC and PANC-1 cells are human pancreatic cancer cell lines (from ATCC). 293T was purchased from ATCC. mCAFs were generated from C57BL/6J harbouring mouse PDAC. hPDAC and hCAFs were generated from PDAC patients.
Authentication	Primary mouse PDAC lines 14837T and 14838T were verified by genotyping. CAFs were verified by measuring α-SMA expression. hPDAC were verified by WB of CK19. All commercially available cell lines were analyzed by STR analysis.
Mycoplasma contamination	all cell lines are negative for mycoplasma contamination
Commonly misidentified lines (See ICLAC register)	no commonly misidentified cell lines were used in the study

Animals and other organisms

Policy information about studies involving animals; ARRIVE guidelines recommended for reporting animal research

Laboratory animals	Six-week-old C57BL/6J mice (male/female) were used for tumorigenesis. Mice for fibroblast deletion of NUFIP1 or ATG5 were generated by breeding NUFIP1fl/fl mice and ATG5fl/fl with FSP-Cre mice (Model Organisms Centre, Shanghai). NUFIP1fl/fl mice were ordered from Cyagen Biosciences (Suzhou, China). ATG5fl/fl mice were ordered from Shanghai Model Organisms Center (ShangHai, China). Mice (male/female) received standard chow diet ad libitum and were housed in conditions of 12/12 h dark/light cycle, 22±1°C ambient temperature and 50±10% humidity at Peking University Health Science Center animal facility. Sex was not considered in our study design. Maximal tumor burden (10% of body weight) and maximal tumor size (2.0cm) allowed by the ethics committee was not exceeded.
Wild animals	the study did not involve wild animals
Field-collected samples	the study did not involve samples from the field

Ethics oversight	All animal experiments were performed in accordance with a protocol approved by the Department of Laboratory Animal Science of Peking University Health Science Center and supervised by the institutional review board of Peking University.

Note that full information on the approval of the study protocol must also be provided in the manuscript.

Human research participants

Policy information about studies involving human research participants

Population characteristics	The primay tumor cell lines, hCAFs, human TMA samples were collected from PDAC patients(male/female) from 34-82 years old diagnosed with PDAC at department of pancreatic surgery, Huashan Hospital.
Recruitment	PDAC patients who received pancreaticoduodenectomy/total pancreatectomy/distal pancreatectomy surgery were recruited into the study. Eligibility criteria for selection of the patients: 1. Encountered between June 2019 and December 2020 2. Age is not limited 3. Underwent surgical therapy and histologically diagnosed postoperatively by two experienced pathologists 4. In accordance with TNM staging system in PDAC of 8th edition AJCC/UICC Classification of Malignant Tumors 5. Tumor tissues of stage IV were confined to those patients who underwent palliative surgery with isolated or single segmental liver metastasis
Ethics oversight	All manipulations about human patient samples were approved by the Research Ethics Committee of Huashan Hospital, Fudan University(protocol number: KY2020-015). All patients provided written informed consent before enrollment and have consented to the data reporting provided in Supplementary Table 4.

Note that full information on the approval of the study protocol must also be provided in the manuscript.